Received: 16 March 2021 | Revised: 1 July 2021 | Accepted: 5 July 2021

DOI: 10.1002/dvdy.394

PATTERNS & PHENOTYPES

Developmental Dynamics WILEY

Published in tribute to the life and scientific achievements of Dr. John F. Fallon.
Article invited by Dr. Matt Harris, Harvard Medical School.

Time-sequenced transcriptomes of developing distal mouse limb buds: A comparative tissue layer analysis

Marc Fernandez-Guerrero[1] | Sofia Zdral[1] | Alejandro Castilla-Ibeas[1] | Lucille Lopez-Delisle[2] | Denis Duboule[2,3,4] | Marian A. Ros[1,5]

[1]Instituto de Biomedicina y Biotecnología de Cantabria, IBBTEC (CSIC-University of Cantabria-SODERCAN), Santander, Spain

[2]School of Life Sciences, Federal Institute of Technology, Lausanne, Switzerland

[3]Department of Genetics and Evolution, University of Geneva, Geneva, Switzerland

[4]Collège de France, Paris, France

[5]Facultad de Medicina, Departamento de Anatomía y Biología Celular, Universidad de Cantabria, Santander, Spain

Correspondence
Marian A. Ros and Denis Duboule, Department of Genetics and Evolution, University of Geneva, 1211 Geneva, Switzerland.
Email: marian.ros@unican.es (M.R.) and denis.duboule@epfl.ch (D.D.)

Funding information
Ministerio de Ciencia e Innovación, Grant/Award Number: BFU2017-88265-P; Swiss National Research Fund, Grant/Award Number: 310030B_138662; ERC grant RegulHox, Grant/Award Number: 588029

Abstract

Background: The development of the amniote limb has been an important model system to study patterning mechanisms and morphogenesis. For proper growth and patterning, it requires the interaction between the distal sub-apical mesenchyme and the apical ectodermal ridge (AER) that involve the separate implementation of coordinated and tissue-specific genetic programs.

Results: Here, we produce and analyze the transcriptomes of both distal limb mesenchymal progenitors and the overlying ectodermal cells, following time-coursed dissections that cover from limb bud initiation to fully patterned limbs. The comparison of transcriptomes within each layer as well as between layers over time, allowed the identification of specific transcriptional signatures for each of the developmental stages. Special attention was given to the identification of genes whose transcription dynamics suggest a previously unnoticed role in the context of limb development and also to signaling pathways enriched between layers.

Conclusion: We interpret the transcriptomic data in light of the known development pattern and we conclude that a major transcriptional transition occurs in distal limb buds between E9.5 and E10.5, coincident with the switch from an early phase continuation of the signature of trunk progenitors, related to the initial proximo distal specification, to a late intrinsic phase of development.

KEYWORDS

AER, *Hox* genes, limb patterning, limb progenitors, RNA-seq, signaling, transcriptome

1 | INTRODUCTION

The basic developmental plan of the tetrapod limb consists of three main segments separated by joints. From the body wall to the distal tip, they are referred to as the stylopod (arm, thigh), the zeugopod (forearm, calf) and the autopod (hand, foot). The stylopod and the zeugopod contain one and two skeletal elements, respectively, whereas the distal segment or autopod contains the multiple skeletal elements of the hand and foot including digits and toes. This basic morphological organization is

Marc Fernandez-Guerrero, Sofia Zdral, and Alejandro Castilla-Ibeas have contributed equally to this study.

highly conserved across species despite the considerable evolutionary variation of the hand/foot that adapted to the multiple, environment-driven activities of the limb.

During limb development, these three limb segments form progressively, in a proximal to distal sequence, under the influence of the Apical Ectodermal Ridge (AER), a thickened epithelium that rims the distal edge of the growing limb bud and is characterized by the expression of several members of the Fibroblast growth factor (Fgf) family, of which Fgf8 is critical.[1] The crucial function of the AER was first revealed long ago by the classical removal experiments performed in the chick embryo by Saunders and collaborators.[2] Removal of the AER produced terminally defective limbs where the level of truncation precisely correlated with the stage when the AER had been removed.[2-4] These experiments revealed for the first time that the limb segments formed progressively, in a proximo-distal (PD) sequence and established the AER as an inductor tissue essential for limb development, contrary to the common assumption at that time that the ectoderm was merely a passive and protective structure.

In order to accommodate the results of the AER removal experiments and thus to explain how various mesodermal cells acquire their proper proximo-distal information, Wolpert and colleagues proposed the "progress zone model".[4] This model posits that distal, subapical mesoderm cells acquire progressively more distal positional values as a factor of the time spent under the influence of the AER in the most distal mesenchymal region called the "progress zone" (PZ). However, the thickness of the PZ has not been precisely defined and, although several genes exhibit expression domains reminiscent of the PZ, amongst them *Msx1*, *Nmyc*, and *Tfap2a*,[5] a reliable and standard PZ marker is still currently unavailable.

The PZ model has been re-assessed several times and the mechanisms and models whereby mesenchymal limb progenitor cells acquire progressively more distal fates are still subject to investigation and debate.[6-8] Studies in chick embryos support a "signal-time model",[6] where the specification of the proximal limb segment depends on signaling from the embryonic trunk, whereas the specification of the distal segments depends on the activation of an intrinsic timing program that starts once the distal limb progenitors are free of proximal signals due to the growth of the bud.[6,9,10] This intrinsic program involves the progressive transition from a proximal to a distal mode of *Hox* gene expression[6,11] that has recently been proposed to be regulated by a proximo-distal gradient of Meis proteins under the control of FGF signaling coming from the AER.[7] However, transcript signatures acquired over time and characteristic of progressively more distal limb progenitor cells have not yet been reported.

Classical tissue recombination experiments showed that the limb bud AER of different developmental stage were functionally equivalent.[12,13] When the ectoderm and mesoderm either from different stages, from various limb types or even from different species were interchanged, limb development continued following the dynamics and origin of the mesoderm compartment.[14,15] These results were interpreted as the AER exerting a permissive role during limb development. However, the analysis of several *AER-Fgfs* mouse mutants showed that the Fgfs released by the AER cells regulate the transcription of the proximo-distal regulators *Meis1* and *Meis2*, suggesting instead an instructive role over the underlying mesenchyme.[16]

Here, to better understand the connections between the AER and the underlying limb progenitors, we set out to determine their gene expression profiles, separately but simultaneously, during critical stages of limb development. We thus generated temporal series of transcriptomes of the AER and try to integrate the datasets with those of the underlying mesenchyme, microdissected at the same stages. We report that a major transition in transcriptional activity occurs in distal limb buds between E9.5 and E10.5, coincident with the switch from an initial signaling activity, related to an early phase of proximo distal specification, to a late intrinsic phase of development. This major change is observed both in the ectoderm and in the mesoderm indicating a parallelism in transcriptional dynamics that fits with the strong connection between both layers. We provide some insights into the expression changes associated with the morphogenetic capacity of limb progenitors and the interaction with the distal ectoderm. Finally, our analysis also identifies transcripts with as yet unknown role in limb development such as *Fgf3*, *Rprm*, and components of the Pdgfa and Hippo signaling pathways whose functional implication remains to be characterized.

2 | RESULTS AND DISCUSSION

2.1 | Temporal series of distal limb transcriptomes from progenitor cells and the overlying ectoderm

To identify gene expression differences that could be involved in the acquisition of progressive PD fates, we generated the transcriptomes of both distal forelimb progenitor cells and the overlying ectoderm at four stages of mouse limb bud development. Due to the progressive PD growth of limb buds, the analysis was restricted to the

distal 150 μm; an approximation of the progress zone[4] guided by previous fate mapping experiments in chick.[6,17,18] The 150 μm thick distal stripe was dissected along with the AER and the two layers were separated by a mild trypsin digestion (Figure 1A and Experimental Procedures). The isolated mesoderm and ectoderm compartments were collected and processed separately. Two biological replicates were collected per stage and each ectoderm and mesoderm replicate were obtained from the same batch of embryos.

This approach had two main advantages. First, it enriched for the pool of undifferentiated progenitors known to be positioned under the AER. Second, it permitted the identification of the ectodermal specific features. Thus, while many bulk transcriptomic studies of the limb bud have been published (ie, [19-21]), these generally included the whole limb bud and hence they contained a heterogenous mix of specified and fully differentiated cells. In these studies, it was also difficult to identify and separate the ectodermal component, as it only accounts for a very small proportion of the cells in the bud. While recent single cell transcriptomics approaches allowed for a clear distinction between ectoderm and mesoderm cells,[22,23] our combination of bulk RNA-seq with fine dissection to study different populations with low noise and high sequencing coverage remains valuable and informative.

We selected four different stages, E9.5, E10.5, E11.5, and E12.5, which together span a wide period of limb development and cover most of key morphogenetic events. The E9.5 stage captures the early initiation of the limb bud. At this time, the AER is forming but has not yet acquired its mature morphology and position. The E10.5 stage is an intermediate stage with a relatively symmetrical bud rimmed by a morphologically mature AER. The E11.5 stage is characterized by the flattened and paddle shaped hand plate in which digits condensations start.[24] To incorporate further temporal information, we also included stage E12.5 with clearly discernible digit condensations and the proximal phalanges being formed.[24] During E12.5 the regression of the AER has already started in a discontinuous manner. While it becomes undetectable over the interdigital spaces, it still remains over the digit tips.[25]

Sequencing libraries were prepared from mRNAs of each of the 16 collected samples and sequenced with 100-bp single-end read length resulting in an average of at least 12 million reads per sample. Nearly 86% of the reads mapped to unique loci and about 11 000 ensembl ids (hereafter referred as genes) per sample were expressed (FPKM above 1). Of the 53 837 genes present in the gtf file, 13 651 (25%) were expressed in at least one of our samples. Of the 21 773 annotated protein coding genes, 12 572 (58%) were expressed in at least one of our samples. Thus, more than half of the annotated protein coding genes in the mouse genome are deployed during the developing distal limb.

These transcriptomic profiling datasets were previously used to explore in details the expression of *Hoxc* genes in the limb bud ectoderm[26] (accession no. GSE150702). We thus used these genes to control the accuracy of the transcriptional profiles during limb development, with respect to both the time and the tissue layer, as well as by the absence of significant cross-contamination between the ectoderm and the mesoderm samples.[26] In this study, we analyze these transcriptomes more globally, using exclusively protein coding genes to try to uncover important differences in gene expression, which would accompany both the PD patterning events during limb growth and the concomitant and necessary mesoderm-ectoderm interactions.

When all samples were analyzed together, the Principal Component Analysis (PCA) expectedly showed that the highest amount of variability (77%) separated the samples by tissue (mesoderm or ectoderm), whereas the second principal dimension (12%) separated the samples by stage (Figure 1B). Because the two biological replicates for each condition clustered well together, indicating biological reproducibility and statistical robustness, a third replicate was not considered necessary.

The second component separated the samples by stage. In this axis, the plot showed that the transcriptional changes between E9.5 and E10.5 were more noticeable than those between E10.5 and E12.5, both in the ectoderm and mesoderm samples. This revealed a major transcriptional switch between E9.5 and 10.5, likely reflecting the continuous interaction between the two limb components. In addition, the limited/reduced variance that separated samples by stage (12%) compared with the separation by tissue (77%), indicated that within each embryonic layer, an important part of the transcriptome is shared throughout the time course analyzed. Interestingly, a prominent transcriptional gap between these two stages (E9.5-E10.5) is also detected in the whole embryo by scRNA-seq.[22]

As expected, when the top 50 (positive X axis) and bottom 50 (negative X axis) with higher impact on the PC1 variance were considered and plotted in a heatmap, most of the top 50 were expressed in the mesoderm layer (Figure 1C) whereas most of the bottom 50 were expressed in the ectoderm layer. The top 50 included genes characteristic of the limb bud mesoderm such as *Fgf10, Prrx1, Twist1, Hand2*, and several *Hox* genes. It also included several genes encoding for hemoglobin chains, which correlated with the presence of the blood

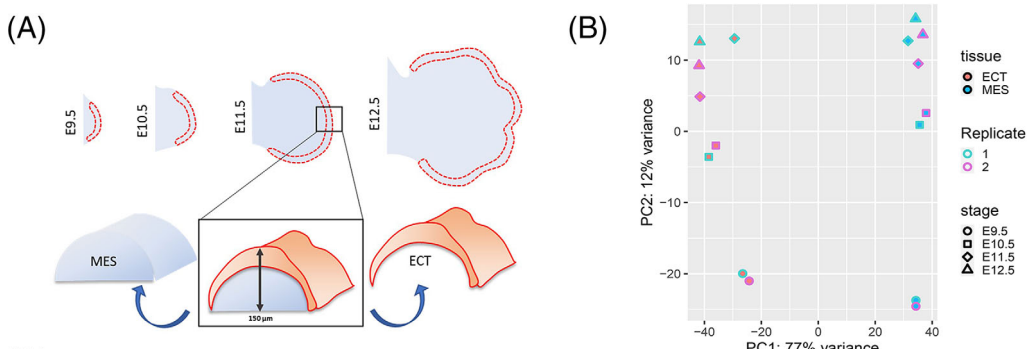

(C)

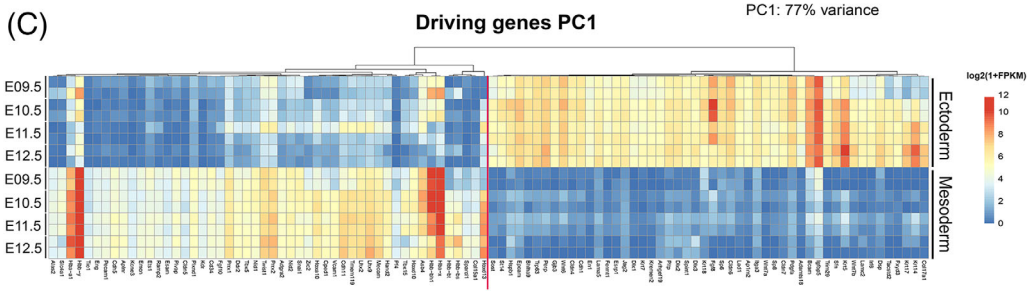

(D)

Enriched terms in top 50 genes from PC1

GO Biological Process	
GO:BP Term	**p-value**
Angiogenesis	0.000
Blood vessel development	0.000
Regulation of angiogenesis	0.000
Appendage morphogenesis	0.000
Limb morphogenesis	0.000
GO Molecular Function	
GO:MF Term	**p-value**
Oxygen carrier activity	0.000
Haptoglobin binding	0.000
Hemoglobin binding	7.98E-12
Oxygen binding	1.22E-11
Peroxidase activity	2.23E-09

Enriched terms in bottom 50 genes from PC1

GO Biological Process	
GO:BP Term	**p-value**
Morphogenesis of an epithelium	0.000
Epidermis development	0.000
Skin development	0.000
Epithelium development	2.01E-15
Epithelial cell differentiation	2.30E-10
Go Molecular Function	
GO:MF Term	**p-value**
Structural molecule activity	6.53E-08
Cell adhesion molecule binding	9.86E-07
Frizzled binding	2.24E-04
Receptor ligand activity	7.10E-04
Laminin binding	3.26E-03

(E)

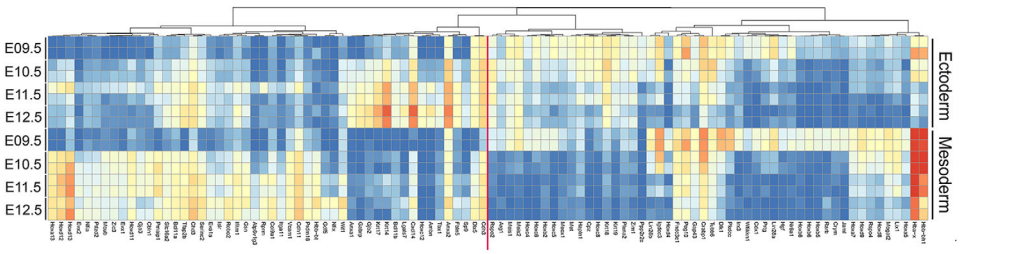

(F)

Enriched terms in top 50 genes from PC2

GO Biological Process	
GO:BP Term	**p-value**
Appendage morphogenesis	9.79E-10
Limb morphogenesis	9.79E-10
Appendage development	3.31E-09
Limb development	3.31E-09
Embryonic limb morphogenesis	1.50E-07
GO Molecular Function	
GO:MF Term	**p-value**
Double-stranded DNA binding	1.41E-07
Sequence-specific DNA binding	2.08E-07
DNA-binding transc. act. activity, RNA pol II-spec.	9.31E-07
Double-stranded DNA helicase activity	3.64E-06
DNA binding	6.60E-06

Enriched terms in bottom 50 genes from PC2

GO Biological Process	
GO:BP Term	**p-value**
Skeletal system development	0.000
Regionalization	0.000
Pattern specification process	0.000
Anterior/posterior pattern specification	0.000
Skeletal system morphogenesis	0.000
Go Molecular Function	
GO:MF Term	**p-value**
DNA-binding TF activity, RNA pol II-specific	0.00E+00
Double-stranded DNA binding	2.86E-11
Sequence-specific DNA binding	4.64E-11
Transcription regulator activity	2.57E-10
RNA pol II reg. region seq. specific DNA binding	2.94E-09

FIGURE 1 Analysis of the temporal transcriptome of the distal limb progenitors and overlying ectoderm. (A) Schematic representation of the procedure followed for sample collection. The distal band dissected for the analysis is delineated in red (top row). The separation between the mesoderm and ectoderm is shown below. (B) Principal component analysis (PCA) plot using the log2(1 + FPKM) values of the 500 most variable protein coding genes. PC1 separates the samples by tissue and PC2 by stage, these components explain 77% and 12% of the variance, respectively. (C) Heatmap showing the log2(1 + FPKM) values of the top 50 and bottom 50 PC1 driving genes. (D) Gene ontology analyses showing five out of the top 20 terms in Biological Process and Molecular Function categories for top 50 (left) and bottom 50 (right) PC1 driving genes. Note that the majority of top 50 PC1 genes are expressed in the mesoderm samples and poorly expressed in the ectoderm samples and vice versa for the bottom 50 PC1 genes. (E) Heatmap showing the log2(1 + FPKM) values of the top 50 and bottom 50 PC2 driving genes. (F) Gene ontology analyses showing five out of the top 20 terms in Biological Process and Molecular Function categories for top 50 (left) and bottom 50 (right) PC2 driving genes

vessels in the subAER mesoderm. It is worth mentioning here that the avascular zone (100 ± 20 μm) observed under the ectoderm of the limb bud in chick is not observed in mouse where blood vessels run immediately underneath the AER. Conversely, the bottom 50 genes driving PC1 were preferentially expressed in the ectoderm layer. Amongst them were the best markers of limb ectoderm and of the AER including *Fgf8, En1, Sp6, Sp8, Wnt6*, and *Jag2*, as well as genes coding either for epithelial structural proteins such as keratins (Krts), that is, *Krt5* and *Kr14* or for cellular adhesion proteins such as cadherins and laminins (Figure 1C and "Global_PC1_with_FPKM_values.xlsx" in Additional files).

Accordingly, the Gene Ontology (GO) analysis of the top 50 genes driving PC1 (associated to tissue factor) showed a significant enrichment in GO Biological Process (BP) terms related to limb morphogenesis and angiogenesis ("angiogenesis", "blood vessel development" and "limb morphogenesis"). GO Molecular Function (MF) related to blood cell function ("oxygen carrier activity" and "haptoglobin binding") were also prominent (Figure 1D). On the other hand, the bottom 50 genes driving PC1 showed a significant enrichment in GO:BP related to epithelial development ("morphogenesis of an epithelium" and "epithelium development") and GO:MF related to epithelia function ("structural molecule activity" and "laminin binding") (Figure 1D).

When the top 50 and bottom 50 genes driving PC2 (associated to developmental time) were considered (Figure 1E), we noticed a large number of *Hox* genes included. The GO analysis retrieved enrichment in GO: BP terms typical of limb morphogenesis ("appendage development" and "limb development") in the top 50 and skeletal development and patterning ("skeletal system development" and "pattern specification process") in the bottom 50 (Figure 1F). GO:MF terms typical of transcription factors/cell identity such ("sequence-specific DNA binding" and "Double stranded DNA binding") were salient in both sets of top and bottom PC2 driving genes (Figure 1F and "Global_PC2_with_FPKM_values.xlsx" in Additional files). The abundance of *Hox* genes included in these top and bottom 50 list, reflect their step-wise activation along with limb PD specification.[11]

Therefore, not unexpectedly, this global analysis showed that the major transcriptomic differences that separated the mesoderm and ectoderm samples corresponded to the expression of tissue specific genes. Amongst them, genes related to the differentiation of the epidermis and of mesodermal specific cell types such as those related to angiogenesis. This analysis also showed that the transcriptomic differences across developmental time were chiefly driven by well-known transcription factors, such as *Hox* genes for example.

2.2 | Differentially spliced exons between ectoderm and mesoderm

Bulk RNA-seq dataset offer full-length transcript coverage allowing for the analysis of the prevalence and potential implications of alternatively spliced transcripts. Indeed, our data permits the separate analysis of differential isoform expression between the ectoderm and the mesoderm during limb development. In mammalian genomes, it has been estimated that nearly all genes can undergo alternative splicing, a process that could in theory dramatically increase the arsenal of transcripts and of potential functions carried by a single gene.[27]

In order to explore the differential exon usage between ectoderm and mesoderm cells we applied the DEXseq R package[28] to our data. DEXseq uses a Generalized Linear Model for each gene to fit the difference in expression across conditions of every exonic part that comprises the gene's isoforms, accounting for every alternative boundary based on a given transcript database. This analysis extracted 1422 differentially used exonic parts between the ectoderm and mesoderm at least in one stage (a 0.5% of 285 926 total exonic parts retrieved), of which 731 exonic parts were enriched in the ectoderm and 691 in the mesoderm. These exonic parts correspond to 1320 merged exons from 1693 transcripts of 644 genes (Figure 2A) (for the complete list refer to "DEexonicparts_pc.xlsx" in Additional files).

While an in-depth analysis of alternative splicing is beyond the scope of this manuscript, to validate our data we show the significant differential exon usage of *Fgfr2* between the MES and ECT samples. As can be seen in Figure 2B, the exonic part 17, corresponding to exon 8, is exclusively found in the ectoderm while the exonic part 16, corresponding to exon 9 is exclusive expressed in the mesoderm. This confirms previous results showing specific expression of Fgfr2 isoform IIIb in ectodermal cells and Fgfr2 isoform IIIc in mesoderm precursors (Figure 2B). This mutually exclusive exon usage between the two tissue layers is the reason why ectodermal cells preferentially respond to Fgf10, whereas mesodermal cells respond to Fgf8.[29] Thus, our datasets offer the possibility of analyzing differential exon usage during limb development.

2.3 | Temporal dynamics of distal limb bud progenitors' transcriptomes

To evaluate the relationships between the expression profiles of limb progenitor cells over time, we performed a PCA only considering the mesoderm samples (Figure 3A). When plotted along the first two components and in two

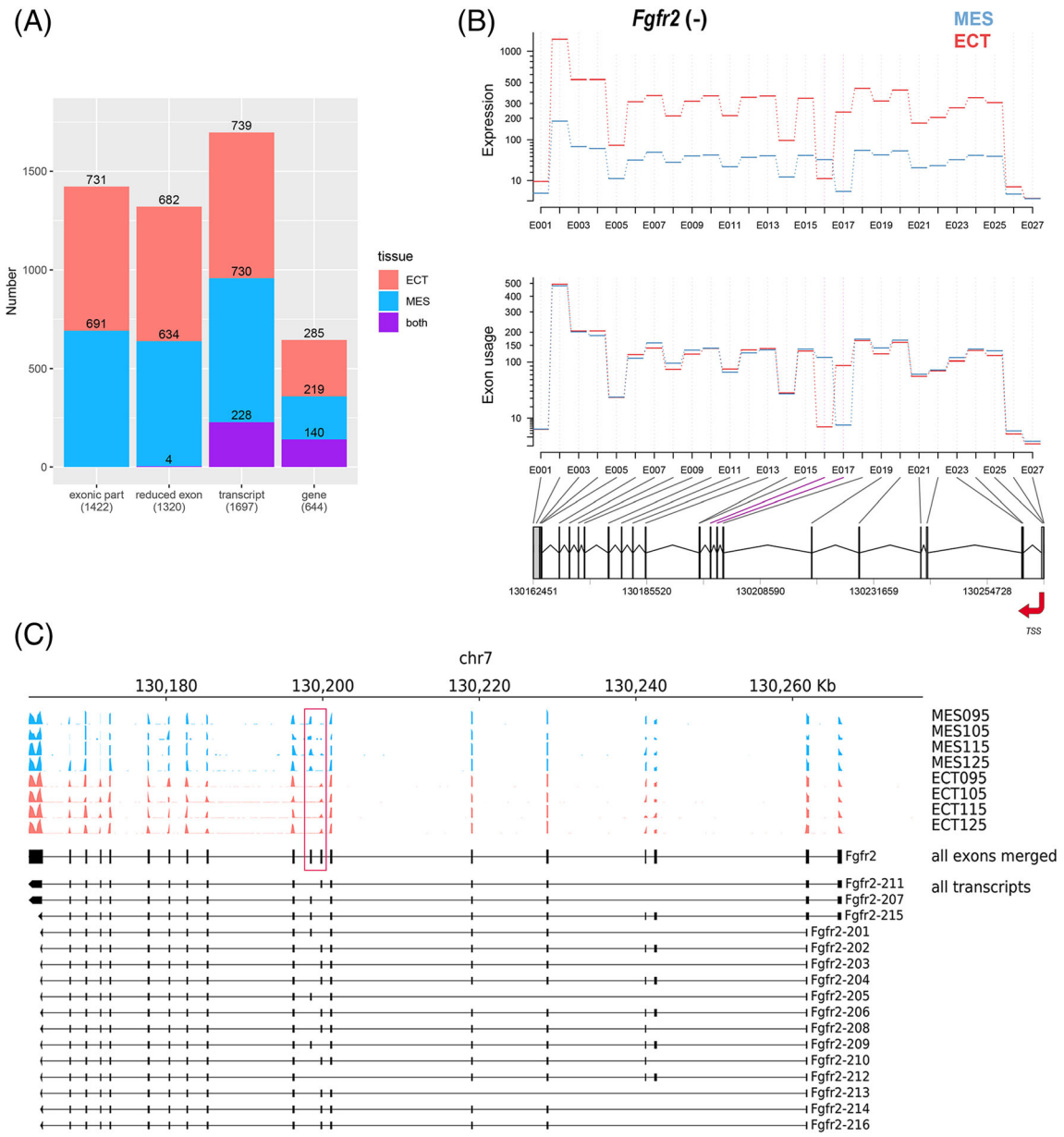

FIGURE 2 RNA-seq differential exon usage between ectoderm and mesoderm. (A) Differential exon usage. Barplot showing the number of exonic parts, merged exons, transcripts and genes with at least one exonic part differentially used between the ectoderm (ECT) and mesoderm (MES) samples. The number of annotations that show at least one exonic part enriched either in the mesoderm, ectoderm, or both (at least one enriched in each tissue) is also shown. (B) Differential usage of unique exons from the *Fgfr2* locus. The graphs show the expression of each exonic part as well as the differential usage of exonic part 16 and 17 between the mesoderm and ectoderm samples. The exonic parts highlighted in purple represent significant differential exon usage. Note that exonic part 17 is practically restricted to the ectoderm whereas exonic part 16 is practically restricted to the mesoderm. (C) Expression profiles of the *Fgfr2* gene in the four stages analyzed. Data were normalized to the million uniquely mapped reads and mean of duplicates is presented. Note that exon 8 corresponding to exonic part 17 is only detected in the ectoderm samples while exon 9 corresponding to exonic part 16 is only detected in the mesoderm samples (red frame)

dimensions, the first dimension (PC1), accounting for 72% of the variance, clearly separated the samples by stage. The second dimension, accounting for 20% of the variance revealed the specificity of the E10.5 transcriptional signature, which appeared clearly separated from the E9.5 transcriptomes. In this PC2 dimension, the E11.5 samples showed positioned between E10.5 and the early (E9.5) and late (E12.5) stages, which were closer to one another (Figure 3A, "MES_PC1_with_FPKM_values.xlsx" and "MES_PC2_with_FPKM_values.xlsx" in Additional files). The GO analysis of the top 100 genes driving PC1 identified GO:BP terms related to skeletal development and

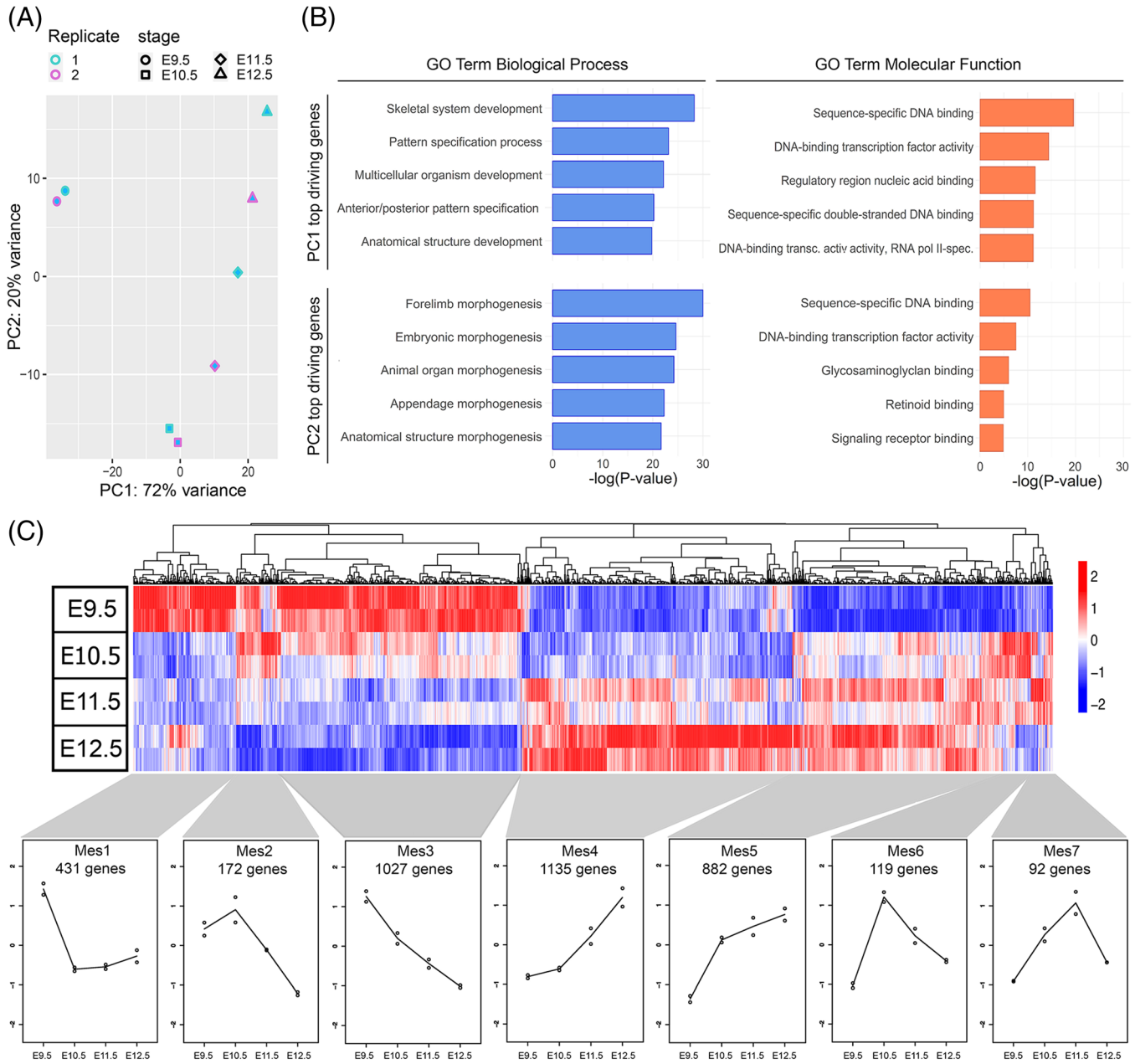

FIGURE 3 Temporal dynamics of mesodermal gene expression. (A) Principal component analysis (PCA) plot of the 500 most variable protein coding genes (FPKM values) in the mesoderm samples. PC1 separates the samples by stage (72% of the variance). PC2 (12% of the variance) unveils the proximity between E9.5 and E12.5 samples. (B) Gene ontology analysis of the PC1 and PC2 top 100 driving genes showing five out of the top 20 terms in Biological Process and Molecular Function categories. (C) Hierarchical clustering (Pearson correlation coefficient) with heatmap (scaled and centered) of the expression profile of MES-DEGs in log2(1 + FPKM). According to the temporal dynamics of expression, seven clusters were extracted and named Mes1 to Mes7 by their order of appearance from left to right in the heatmap. A line chart with the mean values of the genes contained in each cluster is depicted at the bottom

patterning ("skeletal system development" and "pattern specification process") and GO:MF terms related to DNA binding functions ("sequence-specific DNA binding" or "DNA-binding transcription factor activity"), suggestive of high transcriptional activity (Figure 3B). As expected, this enrichment of terms was comparable to those in the PC2 when all samples were analyzed (Figure 1D). Amongst the GO:BP terms enriched in the PC2 top gene list in the mesoderm samples, those related to limb morphogenesis were salient ("forelimb morphogenesis", "appendage morphogenesis") and amongst the GO:MF terms, there was an enrichment in functions associated with growth factor signaling pathways ("glycosaminoglycan binding", "sulfur compound binding", "heparin binding" and "retinoic

binding") consistent with the specific activation of a set of signaling pathways being involved in the large transcriptional variations observed along PC2 (Figure 3B).

To gain insight into the gene regulatory networks regulating the progressive specification of the limb along the PD axis, we examined the temporal pattern of changes in gene expression in distal limb progenitors. We extracted the differentially expressed genes (DEGs) in the mesoderm samples using DESeq2, with a Likelihood Ratio Test (LRT) on all the mesoderm samples. Genes with an adjusted *P*-value below .05 were considered as significantly differentially expressed. The resulting 3858 DEGs in the mesoderm samples (MES-DEGs) were submitted to hierarchical clustering and grouped into seven clusters, according to their temporal expression profiles. The clustered heatmap with the seven clusters, termed Mesodermal clusters 1 to 7 (Mes1 to Mes7), as well as the plots of expression profiles are shown in Figure 3C. The temporal dynamics in the expression profiles in different clusters showed either an stark initial drop and subsequent maintenance in Mes1 (431 genes), a slight initial increase followed by a steady decline in Mes2 (172 genes), a steady decline in Mes3 (1027 genes), a small initial increase followed by significant increase in Mes4 (1135 genes), a robust initial increase followed by a modest increase in Mes5 (882 genes), and inverted V profiles peaking either at E10.5 in Mes6 (119 genes) or at E11.5 in Mes7 (92 genes). The list of genes for each cluster can be found in "MES_clusters_with_FPKM_values.xlsx" in Additional files.

Since this clustering analysis reflects genes sharing comparable expression dynamics, it may reveal potential gene networks regulating important transitory processes during limb development. To further examine this possibility, the list of genes belonging to each cluster was subject to GO terms enrichment analysis and five of the 20 most represented terms in the GO:BP and GO:MF categories are shown in Table 1 (see also "MES_and_ECT_clusters_Enriched_GO_terms.xlsx" in Additional files). This analysis revealed a number of features that can be accommodated with the cluster' trajectories. Briefly, clusters Mes1 and Mes3, both with maximal expressions at E9.5 (Figure 3C), were enriched in terms associated with pattern specification (Mes1) or high transcriptional and metabolic activity (Mes1 and Mes3), both features of undifferentiated and pluripotent cells.[30] Conversely, both Mes4 and Mes5, with trajectories progressively upregulated over time (Figure 3C), showed enrichment in GO:BP terms pointing to cell differentiation ("cell differentiation" and "connective tissue development") and GO:MF terms related to the establishment of the cytoskeleton and the extracellular matrix (ECM) ("ECM constituent" and "cytoskeletal protein binding"), thus connecting these categories to the progressive aging of limb progenitors (Table 1).

The over-representation of GO terms in clusters Mes2, Mes6, and Mes7, peaking at E10.5 or E11.5, respectively, was less significant than in the other clusters probably due to the smaller number of genes included (Table 1). Nevertheless, enriched terms related to modulation of signaling activities ("negative regulation of signal transduction" and "hedgehog receptor activity") clearly emerged in cluster Mes6 (peaking at E10.5). Assigned to these GO categories were genes such as *Spry2*, *Dusp6*, and *Ptch1*, which are well-known targets and negative feedback regulators of Fgf and Sonic Hedgehog (Shh) signaling, indicating the high activity of these pathways in this intermediate stage of limb development.

2.4 | Gene expressions associated with early and late distal limb progenitors

It is well known that distal limb bud progenitors undergo a progressive reduction in their morphogenetic capacity along with development, despite their sustained proximity to the AER.[6,31] To identify genes whose expression dynamics would either positively or negatively correlate with the ageing of these mesoderm cells, we analyzed clusters Mes1 and Mes3, that is, those displaying downward gene expression trajectories, and clusters Mes4 and Mes5, that is, those showing upward gene expression trajectories (Figure 3C).

The presence in clusters Mes1 and Mes3 of genes expressed in undifferentiated cells was noteworthy in this respect (Figure 4A,B). These included the pluripotency-associated genes *Lin28a* and *Lin28b*,[32,33] the early embryonic and stemness regulator gene *Sall4*,[34-36] as well as other regulators of pluripotency such as *Fzd7*.[37] *Lin28* genes have a well-recognized function as regulators of pluripotency.[38] LIN28 proteins are members of an RNA-binding protein family, which function as posttranscriptional regulators involved in developmental timing and self-renewal in embryonic stem cells (reviewed in Tsialikas and Romer-Seibert[32]). While previous expression of *Lin28a* had been described as very broad in the early embryo and limb buds,[39,40] whole-mount in situ hybridization (WMISH) detected *Lin28a* and *Lin28b* expression in early E9.5 forelimbs, yet not in subsequent stages (Figure 4B), in agreement with the expression profiles of genes belonging to clusters Mes1 and Mes3. The RNA-seq showed that the amount of *Lin28a* transcripts declined more rapidly than those of *Lin28b* between E9.5

TABLE 1 Selected GO:BP and GO:MF from the top 20 enriched terms in mesoderm clusters

Cluster	GO BP term	*P* value	GO MF term	*P* value
Mes1	Anatomical structure morphogenesis	3.08E-26	Sequence-specific DNA binding	2.86E-12
	Multicellular organism development	5.58E-25	DNA-binding TF activity	7.97E-12
	Developmental process	1.84E-24	DNA-binding TF activity, RNA pol. II-specific	4.33E-11
	Anterior/posterior pattern specification	2.72E-19	Transcription regulator activity	3.34E-09
	Pattern specification process	1.76E-18	DNA - binding transactivator activity, RNA pol. II-specific	3.39E-07
Mes2	Multicellular organism development	1.52E-07	Binding	5.19E-09
	System development	4.30E-07	Protein binding	1.58E-06
	Anatomical structure development	2.75E-06	LBD domain binding	1.40E-03
	Developmental process	5.04E-06	Nucleic acid binding	1.58E-03
	Cellular component organization	2.47E-05	Organic cyclic compound binding	2.01E-03
Mes3	Ribonucleoprotein complex biogenesis	1.71E-79	RNA binding	3.36E-46
	Ribosome biogenesis	4.52E-76	Catalytic activity, acting on RNA	1.74E-34
	Rrna metabolic process	1.73E-57	Catalytic activity, acting on a trna	1.19E-23
	RNA processing	6.56E-57	Snorna binding	5.74E-15
	Gene expression	1.70E-43	Transferase activity, transferring one-carbon groups	1.03E-13
Mes4	Anatomical structure development	1.51E-27	Protein binding	4.08E-16
	Regulation of cell differentiation	6.72E-25	Calcium ion binding	1.14E-09
	Cell differentiation	4.15E-24	Extracellular matrix structural constituent	7.63E-09
	Tissue development	1.52E-22	Cation binding	2.33E-08
	Connective tissue development	3.49E-19	Metal ion binding	2.76E-08
Mes5	Anatomical structure development	6.15E-17	Cytoskeletal protein binding	6.84E-11
	Movement of cell or subcellular component	2.77E-15	Actin binding	2.01E-07
	Cell differentiation	2.66E-14	Actin filament binding	2.08E-06
	Cellular developmental process	5.60E-14	Phospholipid binding	1.08E-05
	Cell morphogenesis	1.72E-13	Microfibril binding	1.37E-04
Mes6	Anatomical structure morphogenesis	1.38E-08	Hedgehog receptor activity	1.14E-04
	System development	3.82E-08	Smoothened binding	1.24E-04
	Negative regulation of signal transduction	4.34E-08	Transmembrane-ephrin receptor activity	1.73E-04
	Negative regulation of cell communication	7.33E-07	Glycosaminoglycan binding	1.89E-03
	Negative regulation of signaling	7.79E-07	Lysophospholipid:sodium symporter activity	3.95E-03
Mes7	Tissue development	7.10E-10	Frizzled binding	4.34E-06
	Animal organ development	1.50E-09	Cadherin binding involved in cell–cell adhesion	1.10E-04
	Multicellular organism development	2.02E-08	Protein binding	6.08E-04
	Anatomical structure development	3.80E-08	DNA-binding TF activity, RNA pol. II-specific	1.53E-03
	System development	5.07E-08	Chromatin binding	1.62E-03

and 10.5 (Figure 4A), thus placing these two genes into two different clusters (Mes1 vs Mes3). However, the *Lin28b* transcripts remaining at E10.5 were under the WMISH detection level (Figure 4B). Transcripts encoded by the *Sall4* gene, also included in cluster Mes3 were detected by WMISH at E10.5 (Figure 4B), likely due to a higher expression level when compared to *Lin28b*.

In contrast, as expected from the GO-term enrichment analysis, genes involved in tissue differentiation were over-represented in clusters Mes4 and Mes5

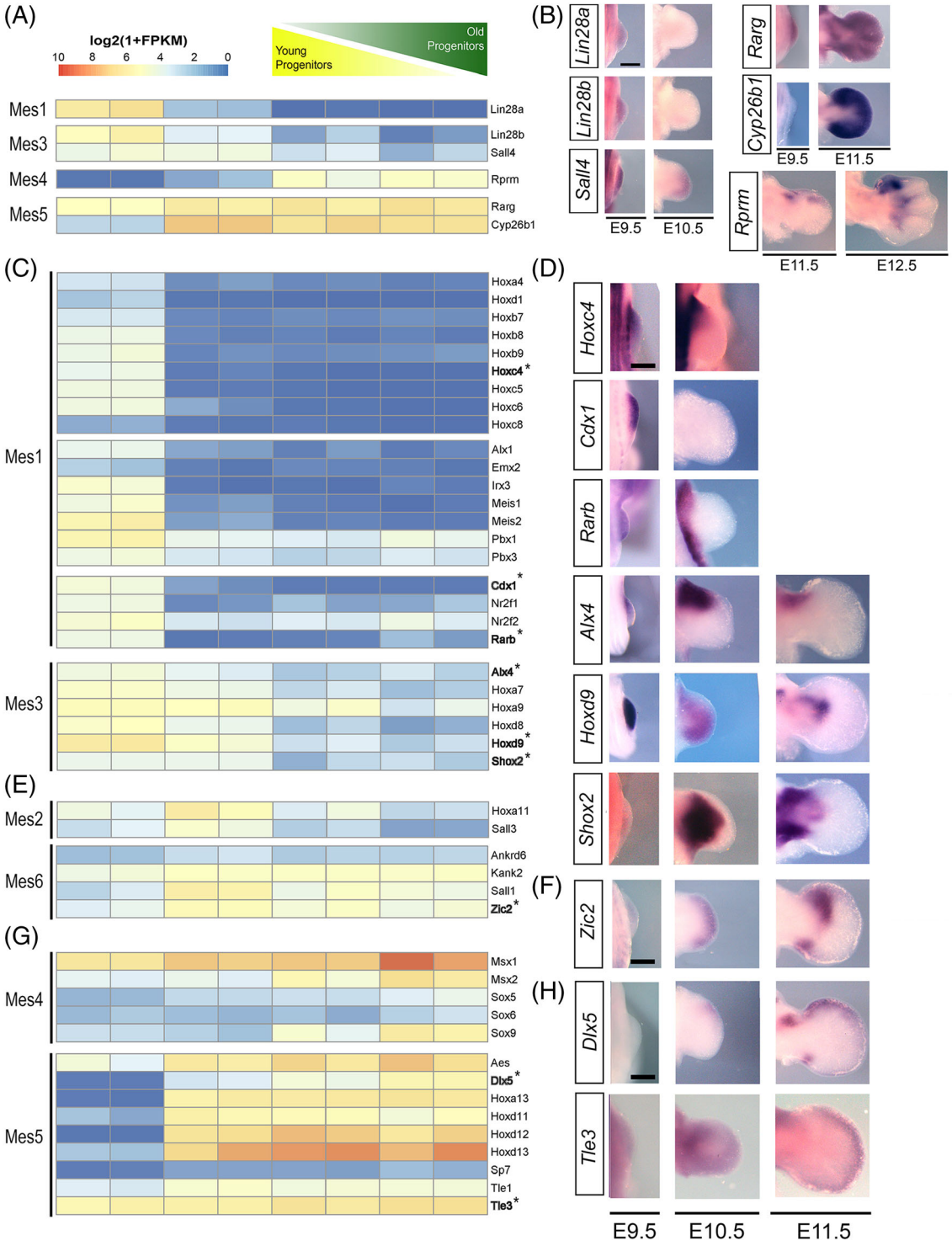

FIGURE 4 Clusters with upward and downwards gene expression trajectories and transcription factor expression profiles. (A) Heatmap with log2 (1 + FPKM) values (A) and WMISH (B) of selected relevant genes associated to early (clusters Mes1 and Mes3) or late (clusters Mes4 and Mes5) limb progenitors. (B) WMISH showing the expression pattern in the stages of interest are steadily upregulated over time and genes in Mes5 experience an initial sudden activation and are subsequently steadily upregulated onwards. (C) Heatmaps of selected relevant transcription factor peaking in E9.5 (clusters Mes1 and Mes3). (D) WMISH showing representative expression patterns of the genes indicated in bold and marked with an asterisk in the heatmaps. (E) Heatmaps of selected relevant transcription factor peaking in E10.5 (clusters Mes2 and Mes6). (F) WMISH showing the expression patterns of *Zic2* as a representative gene of these clusters. (G) Heatmaps of selected relevant transcription factor with maximal expression at E12.5 (clusters Mes4 and Mes5). (H) Expression of *Dlx5* and *Tle3* as representative of these clusters. Note the coherence between the expression pattern and the heatmap profiles. All pictures are dorsal views of limb buds of the indicated stage. Anterior is to the top and distal is to the right. Scale bars are 500 μm

("MES_clusters_with_FPKM_values.xlsx" Additional files). Genes known to regulate chondrogenic differentiation and limb skeletal, digit and joint morphogenesis including *Bmp2, Col2a1, Gdf5*, and *Nog* were present in cluster Mes4, which was characterized by upward trajectories over time, more pronounced from E10.5. Two members of the retinoic acid pathway, *Rarg* and *Cyp26b1*[41] were also identified in cluster Mes5 (Figure 4A,B), probably reflecting their involvement in skeletal patterning.[42]

In support of this, clusters Mes4 and Mes5 contained a large number of structural genes including several collagen genes *(Col1a1, Col5a1, Col9a3, Col24a1, Col4a5, Col12a1, Col16a1, Col6a3, Col8a1*), non-muscle myosins (*Myo1e, Myo1d, Myh9*), integrins (*Itga2, Itga11, Itga6, Itga8*), and *Arhgef* genes(*Arhgef28, Arhgef3, Arhgef9, Arhgef19, Arhgef6, Arhgef26, Arhgef40, Arhgef17, Arhgef5, Arhgef10l, Arhgef37, Arhgef10*). The latter genes code for Rho-guanyl exchange factors involved in the activation of Rho, a major regulator of the cellular actin cytoskeleton.[43,44]

Particularly striking was the presence in cluster Mes4 of the *Reprimo* gene (*Rprm*, assigned to the GO:MF "protein binding" term), a tumor-suppressor gene implicated in p53-mediated cell cycle arrest.[45] As it is known that the ratio of distal progenitors in G1 raises over time,[6] we analyzed its expression pattern during limb development. *Rprm* transcripts were first detected by WMISH at E11.5, indicating expression below detection level at earlier stages (Figure 4A,B). From E11.5 onwards, *Rprm* was detected in the distal-anterior mesoderm and, at 12.5, in the whole digit 1 area and the basis of digits 2 to 4. This polarized and anteriorly restricted expression pattern of *Rprm* does not support a function in controlling the cell cycle of distal progenitors. Furthermore, *Rprm* is thought to function in G2 arrest, while the growth deceleration of limb progenitors is associated with an elongation of the G1 phase.[6,46] However, *Rprm* function in cell cycle has not been completely established[45,47] and an alternative role in cell death control has also been proposed for this gene.[48] Further studies in the developing limb bud system may help clarify these issues.

Collectively, our data show the progressive loss of stemness state and increase in skeletal specification of the distal limb progenitors over time. This is in contrast with the current assumption that the distal mesoderm remains undifferentiated as long as being under the influence of the AER. Amongst the genes that could potentially contribute to the stem cell-like state of the early progenitors, *Lin28* appear as good candidates, as also observed in chick limb buds.[46] A recent study revealed that *Hoxb13* and *Hoxc13* genes terminate the expansion of tail bud progenitors in mice, at least in part by inhibiting the expression of *Lin28* genes.[40] Whether a similar regulatory mechanism between *Hox13* paralogs (in this case *Hoxa13* and *Hoxd13*) and *Lin28* genes occurs during limb bud development, remains open. The progressive activation of the chondrogenic program over time in distal limb mesoderm correlates with the progressive increase in Bmp signaling,[19,46,49] as well as with the progressive loss of AER activity and its concurrent negative effect on the cytodifferentiation of limb mesenchymal cells located underneath.[50]

2.5 | Stage-specific transcriptional signatures of distal limb progenitors

We also asked whether the limb progenitors carry specific transcriptional signatures associated to their proximo-distal states of specification. To identify developmental stage-specific gene expression patterns, we further explored the list of genes with expression profiles peaking at each stage, focusing on TFs as determinants of cellular identity by intersecting the lists of genes in each cluster with a curated set of mouse genes coding for transcription factors[51] ("MES_clusters_with_FPKM_values.xlsx" in Additional files).

Amongst the 76 TFs included in the Mes1 cluster, a large set of *Hox* genes including *Hoxd1*, *Hoxb1* to *9* and several 3′ members of the *HoxA* and *HoxC* clusters stood out (see the heatmap in Figure 4C). The expression of these *Hox* genes was mostly restricted to E9.5 and undetectable subsequently, as shown for *Hoxc4* in Figure 4D. Mes1 also included several TF with well documented roles in the development of the proximal limb, for example the *Irx3,5*,[52] *Meis1,2*,[53,54] *Pbx1,3*,[55] and *Emx2*[56] (Figure 4C). *Meis1* and *Meis2* are well-known markers of the proximal limb segment and inactivation studies have demonstrated their essential function during trunk development and forelimb formation, as well as their involvement in proximo-distal limb patterning.[7,57] *Pbx* and *Emx2* are members of the regulatory networks acting during shoulder girdle development.[56] The expression of these genes in the early E9.5 distal limb bud progenitor cells provide additional validation to our datasets and confirms the stylopod specification state of these progenitors.

Moreover, a set of genes known to be transcriptional targets of Retinoic Acid (RA) in the trunk, including *Cdx1*, *Nr2f1*, *Nr2f2*, and *Rarβ*[57] were also spotted in cluster Mes1 (Figure 4C). *Nr2f1*, *Nr2f2*, and *Rarβ* are nuclear RA receptors (RARs) that bind DNA sequences known as RA response elements (RAREs) as a heterodimer complex with retinoid X receptors (RXRs). *Cdx1* gene is a member of the caudal-related homeobox transcription

factor family involved in growth of embryonic posterior axial progenitors. Interestingly, *Cdx1* is included in all the top 5 GO:BP enriched terms in Mes1 (Table 1). The expression of these RA transcriptional targets in the distal progenitors of the E9.5 forelimb bud (Figure 4D) indicates that RA signaling reaches the distal tip of the early bud and underscores the commonalities between the early limb bud and trunk progenitor cells.

Another group of TFs showing an expression peak at E9.5 were included into cluster Mes3 due to their less abrupt decay than that occurring in the Mes1 cluster (Figure 4C). Amongst those are *Alx3* and *Alx4*, which are markers of the proximal anterior mesoderm, and another set of *3′Hoxa* and *Hoxd* genes including the stylopod-associated genes *Hoxa9* and *Hoxd9* and *Shox2*. As previously reported, the expression patterns of all these genes fit well with their known function in limb development[58] (Figure 4D). *Shox2* and *Hox* genes have related spatial expression dynamics, with *Shox2* expression restricted to the proximal limb along with *Hoxd9* and *Hoxa11*.[59]

In summary, the transcriptional signature of the early (E9.5) limb progenitors is dominated by three predominant features: stylopod-associated markers, RA responsive genes and 3′ *Hox* genes of all clusters. Overall, this signature indicates an extension, in limb progenitors, of the identity of trunk progenitors, from which they derive.[57] It also shows that RA signaling reaches the distal tip of the early bud, an observation further supported by the expression of several RA targets in the early limb bud ectoderm (see below).[60] Some of these factors are abruptly downregulated from E9.5 onwards (Mes1) in the distal limb progenitors, whereas others slowly decline over time (Mes3). Amongst the formers are the stylopod associated genes that remain expressed in the stylopod cells, while in the latter are *Shox2* and *Hox9* paralogs, gradually transitioning to the distal limb bud developmental program.

To analyze the TF coding genes expressed with a peak at E10.5, we focused on clusters Mes2 and Mes6, which contained only 19 and 12 TFs, respectively. Noteworthy, cluster Mes2 contained *Hoxa11*, a known marker for zeugopod cells, which is also highly expressed in E9.5 and peaking at E10.5 (Figure 4E). Other TFs with highest transcript levels at E10.5 included *Sall3* in Mes2, and *Sall1* and *Zic2* in Mes 6 (Figure 4E,F). These latter genes participate in autopod development, in particular *Sall1* and *Sall3* in digit specification through *Hox* gene modulation[61,62] and *Zic2* in the morphogenesis of the wrist and ankle.[63] Accordingly, the temporal WMISH of *Zic2* shows its peaking in E10.5 distal progenitors and posterior restriction to the wrist (Figure 4F). Clusters Mes2 and Mes6 also contained several genes coding for members of the Ankyrin repeat domain protein family (ARDPs) including *Ankrd6*, *Asb4* and *Kank2* (Figure 4E). ARDPs are wide-spread structural proteins mediating protein-protein interactions in all phyla.[64,65] These proteins play a role in processes including transcriptional regulation, cytoskeletal organization and cell cycle progression.[65,66] *Asb4* is expressed in the distal anterior mesoderm and negatively regulated by *Shh*.[67] *Ankrd6* and *Kank2* also show patterns of expression expected for genes belonging to the Mes6 cluster (EMBRYS database of embryonic gene expression.[38,67] Therefore, the analysis of the TFs with maximal expression in E10.5 progenitors confirmed their specification to the zeugopod state. However, the presence in this cluster of other TFs whose perturbations preferentially impact the development of the autopod may reflect a mixture of cells specified for zeugopod and autopod in the distal tip of the E10.5 limb bud or, alternatively, transitional states expressing zeugopod and autopod genes. Single cell analysis would be very helpful to clarify this point.

We then searched for TF coding genes with a maximal expression at E11.5 (Mes7) and found little or no results, except for the *Gli1* and *dHand2* genes whose highest expressions at this stage were interpreted as a consequence of the anterior expansion of their expression domains reflecting progression of AP patterning. We note that several TFs typical of the ectoderm were found in this cluster, revealing a contamination of one of the E11.5 samples. However, this contamination was minimal considering the low expression values observed (highest FPKM = 0.409, corresponding to *Hoxc13* in the mesoderm).

To determine the specific transcriptional signature of late E12.5 progenitors, which are generating the digits[68,69]), we concentrated on the TF coding genes included in clusters Mes4 and Mes5 and identified 128 and 75, respectively. GO:BP enriched terms in these clusters were associated with cell differentiation and specialization (Table 1). Although chondrogenesis or skeletal differentiation was not specifically pointed out in the GO enrichment analysis, a manual revision identified many genes with known role in these processes. Thus, *Sox9*, a major regulator of chondrogenesis, *Sox5*, *Sox6*, *Msx1*, *Msx2*, and the early osteoprogenitor marker *Runx2* (Figure 4C) were found in cluster Mes4 and *Sp7* (*Osterix*) and *Dlx5*[70,71] in Mes5 (Figure 4D). The temporal WMSIH analysis for *Dlx5* corroborated its steady increased expression over time in distal cells (Figure 4H).

Yet the hallmark genes in cluster Mes5 were the most 5′ *Hoxa* and *Hoxd* genes including *Hoxa13*, the best marker of the autopod and *Hoxd11-13*, which are important regulators of digit patterning (Figure 4G). The transcription factor signature of the late limb bud progenitors is thus characterized by the expression of markers of

chondrogenic and osteogenic differentiation and a high expression of 5′ *Hoxa* and *Hoxd* genes, in particular the *Hox13* paralogs. In addition, several members of the transducin-like enhancer of split (TLE) family of transcriptional corepressors (also known as Groucho-related genes) including *Aes* (*Tle5*), *Tle1*, *Tle3*, and *Tle4* were found in cluster Mes5 (Figure 4G,H). Some of these factors function as transcriptional co-repressors to negatively regulate *Wnt* signaling[72] and could thus participate in the *Wnt* dependent modulation of the chondrogenic differentiation in distal cells.[50] The progressive increase in *Tle3* expression level in the distal limb progenitors is observed in the temporal WMISH (Figure 4H).

Consequently, gene-expression signatures of early-phase and late-phase limb progenitors were associated with the first and second phase of *Hox* gene expression.[11] Recently a possible mechanism to link progression in PD specification and *Hox* gene expression has been proposed based on a PD gradient of Meis proteins.[7] In the emerging bud, *Meis* expression correlates with RA signaling. When RA signaling is distally repressed by Fgf-mediated induction of Cyp26b1[16,41,54] the stability of Meis proteins generates a continuous PD gradient that somehow impact the expression of *Hox* genes.[7]

2.6 | Temporal transcriptome dynamics of the distal limb bud ectoderm

To evaluate the relationship between the expression profiles of distal ectodermal cells over the stages analyzed, we performed a PCA including only the ectoderm samples (Figure 5A). Noteworthy, the ectodermal region concerned in this study corresponds to the ectoderm covering the distal 150 μm of the limb bud. This region includes the AER and the flanking dorsal most and ventral most ectoderm (Figure 1A, Experimental Procedures). Within this region, the AER is the predominant component and signaling center and hence this is the cell cluster where important changes in gene expression are postulated to occur.

Similar to the situation with the mesodermal samples, the first dimension (PC1), which accounted for 67% of the variance, separated the samples by developmental stage. The second dimension, accounting for 17% of the variance, distributed the samples in identical pattern as the mesodermal samples, underscoring the singularity of the E10.5 stage and the parallel transcriptional dynamics between the two limb components probably reflecting the strong connection between them (Figure 5A, compare with Figure 3A).

The GO analysis of the top 100 genes driving PC1 identified GO:BP terms related to developmental processes and to RA metabolism ("anatomical structure development" and "RA catabolic process") and GO:MF terms related to TF functions and RA binding ("DNA-binding transcription factor activity" and "RA binding") (Figure 5B and "ECT_PC1_with_FPKM_values.xlsx" in Additional files). The GO:BP terms enriched in the PC2 top gene list were generic and less informative ("appendage morphogenesis", "limb development") while the GO:MF were enriched in terms related to growth factor activity ("growth factor receptor binding" or "growth factor activity") (Figure 5B and "ECT_PC2_with_FPKM_values.xlsx" in Additional files). Therefore, the aging of distal ectodermal cells (PC1) was strongly associated with the progressive removal of RA signaling, whereas the differences between stages (PC2) seemed to rely on the specific patterns of growth factor activity.

2.7 | Gene expression dynamics in the distal ectoderm

To gain insight into the temporal dynamics of AER signaling, we extracted the genes differentially expressed in the various ectoderm samples and used the same pipeline as applied to mesoderm cells. We qualified 2444 genes that were differentially expressed in the ectoderm across stages (ECT-DEGs). The ECT-DEGs ("ECT_clusters_with_FPKM_values.xlsx" in Additional files) were grouped into six clusters according to their temporal expression profiles. The clustered heatmap with the six clusters, termed Ectodermal clusters 1 to 6 (Ect1 to Ect6) and the plots of the expression profiles are shown in Figure 5C. Briefly, the gene expression trajectories in these clusters either followed a steadily increase over time (Ect1; 1069 genes), an initial strong increase followed by maintenance (Ect2; 323 genes), a maxima at E10.5 (Ect3; 224 genes), an initial dramatic decrease followed by maintenance (Ect4; 83 genes), a stable expression followed by an abrupt drop (Ect5; 45 genes) or a steadily decrease (Ect6; 685 genes).

To explore the functional relevance of these trajectories, the list of genes in each cluster was subject to GO analysis. Five out of the 20 over-represented terms are shown in Table 2 ("MES_and_ECT_clusters_Enriched_GO_terms.xlsx" in Additional files). In agreement with the upward profiles displayed in clusters Ect1 and Ect2, the enriched GO terms associated with cell differentiation, maturation of the ECM structure and cytoskeleton, and regulation of adhesive properties ("cell differentiation", "extracellular matrix structural constituent" and "cell adhesion"). The GO analysis in the set of genes in cluster Ect3, whose RNAs were at maximum at E10.5, showed enrichment in GO:BP terms such as "cell surface receptor signaling pathway",

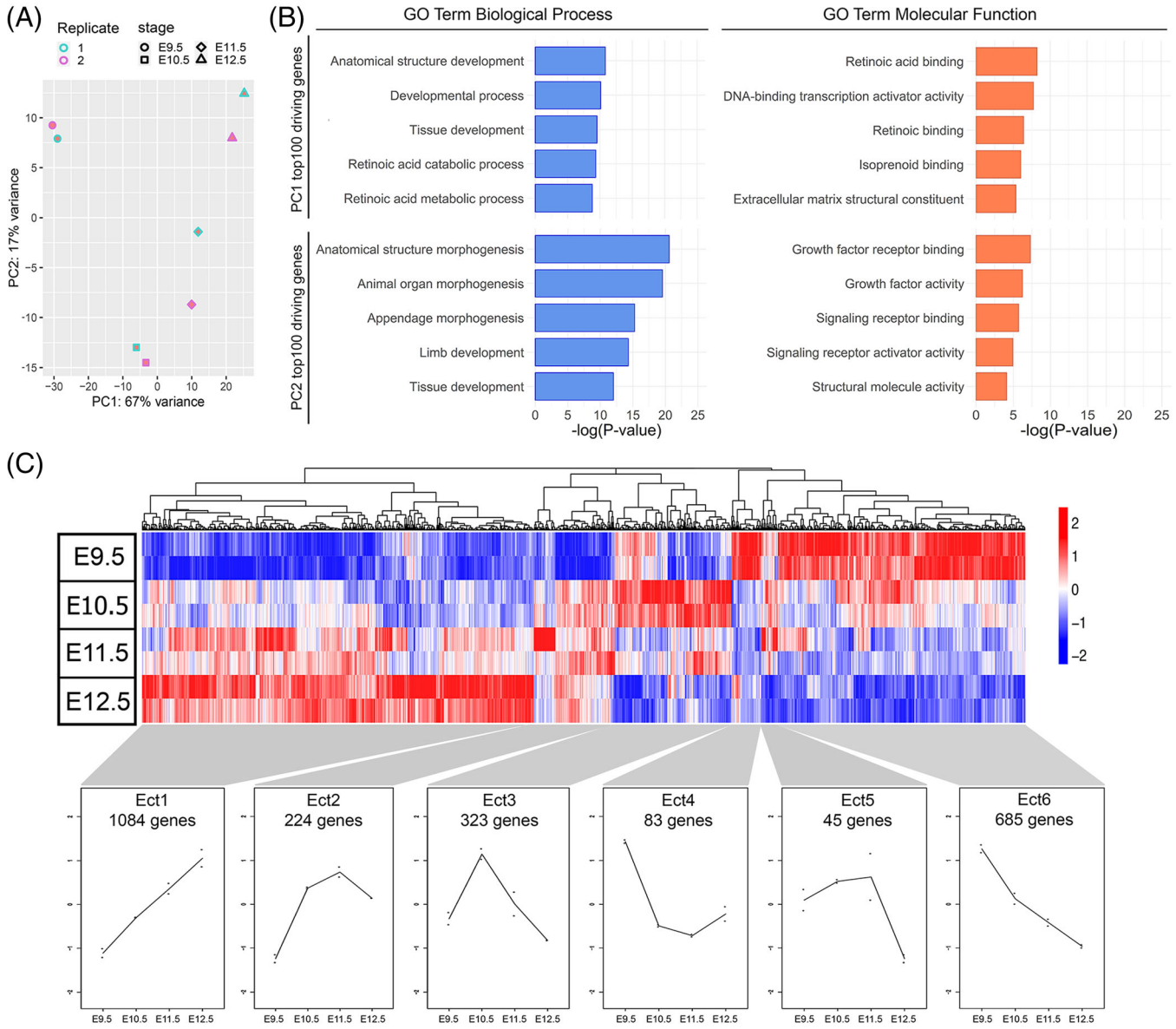

FIGURE 5 Temporal dynamics of ectodermal gene expression. (A) Principal component analysis (PCA) plot of the 500 most variable protein coding genes (FPKM values) in the ectoderm samples. PC1 separates the samples by stage (67% of the variance). PC2 (17% of the variance) distributes the samples following the same pattern as in the mesoderm. (B) Gene ontology analysis of the PC1 and PC2 top 100 driving genes showing five out of the top 20 over-represented GO terms in Biological Process and Molecular Function categories. (C) Hierarchical clustering (Pearson correlation coefficient) with heatmap (scaled and centered) of the expression profile of ECT-DEGs in log2(1 + FPKM). According to the temporal dynamics of expression, six clusters were extracted and named Ect1 to Ect6 by their order of appearance from left to right in the heatmap. A line chart with the mean values of the genes contained in each cluster is depicted at the bottom

"cell-cell signaling" and "signaling receptor binding" reflecting the high signaling activity in the E10.5 limb bud ectoderm. Similarly, GO:MF enriched terms in cluster Ect3 included "fibroblast growth factor receptor binding" and "frizzled binding" matching the expression peak of several AER-*Fgfs* (*Fgf8*, *Fgf4*, and *Fgf17*) and several *Wnt* ligands (*Wnt8a*, *Wnt5a*, *Wnt10b*, and *Wnt10a*), thus providing a potential explanation for the singularity of the E10.5 stage observed in PC2. Cluster Ect4, including genes with maximal expression at E9.5, was enriched in terms related to "stem cell differentiation", "skeletal system morphogenesis" and TF activity. This surprising enrichment in skeletal morphogenesis is driven by the expression of genes with known functions in skeletal patterning such as *Sox9*, *Meis1/2*, and *3′Hox* genes, but whose ectodermal domains are rather linked to the maintenance of pluripotency and RA signaling.[73] Genes in cluster Ect5, steeply decaying from E11.5, associated with appendage morphogenesis and

TABLE 2 Selected GO:BP and GO:MF from the top 20 enriched terms in ectoderm clusters

Cluster	GO BP TERM	*P* value	GO MF TERM	*P* value
Ect1	Anatomical structure morphogenesis	1.64E-30	Extracellular matrix structural constituent	1.96E-11
	Biological adhesion	2.02E-22	Calcium ion binding	6.77E-11
	Cell adhesion	4.88E-22	Cell adhesion molecule binding	3.85E-10
	Cell differentiation	5.35E-20	Structural molecule activity	1.47E-09
	Regulation of cell communication	1.78E-17	Cytoskeletal protein binding	1.73E-06
Ect2	Tissue development	6.10E-11	Protein binding	4.09E-06
	Anatomical structure development	2.90E-09	Calcium ion binding	1.62E-04
	Cell differentiation	3.12E-09	Extracellular matrix structural constituent	6.96E-04
	Cellular developmental process	6.54E-09	Ephrin receptor activity	1.19E-03
	Regulation of cell differentiation	8.35E-08	Transmembrane receptor protein tyrosine kinase activity	1.45E-03
Ect3	Cell surface receptor signaling pathway	6.03E-15	Fibroblast growth factor receptor binding	1.37E-07
	Cell–cell signaling	4.83E-12	Growth factor activity	5.48E-07
	Cellular developmental process	7.04E-11	Growth factor receptor binding	8.13E-07
	Regulation of cell communication	1.45E-09	Signaling receptor binding	4.54E-06
	Regulation of signaling	1.80E-09	Frizzled binding	1.91E-04
Ect4	Animal organ morphogenesis	9.82E-10	Sequence-specific DNA binding	3.44E-08
	Stem cell differentiation	1.39E-09	RNA pol. II transcription regulatory region sequence-specific DNA binding	6.62E-06
	Skeletal system morphogenesis	1.86E-08	Regulatory region nucleic acid binding	1.36E-05
	Developmental process	1.05E-07	DNA binding transcription activator activity, RNA pol. II-specific	2.07E-05
	Embryonic skeletal system development	1.49E-07	Protein binding	2.16E-05
Ect5	Anatomical structure morphogenesis	0.00E+00	RNA pol. II transcription regulatory region sequence-specific DNA binding	1.54E-06
	Embryonic limb morphogenesis	4.35E-11	Transcription regulatory region sequence-specific DNA binding	2.75E-06
	Embryonic appendage morphogenesis	4.35E-11	Regulatory region nucleic acid binding	2.87E-06
	Appendage development	9.85E-10	Sequence-specific double-stranded DNA binding	4.31E-06
	Limb development	9.85E-10	DNA-binding TF activity, RNA polymerase II-specific	3.64E-04
Ect6	Developmental process	7.09E-24	Protein binding	1.43E-15
	Cellular developmental process	1.79E-17	DNA-binding TF activity	2.60E-09
	Cell differentiation	9.71E-17	Ion binding	9.14E-09
	Negative regulation of cellular process	2.58E-16	Catalytic activity	2.27E-06
	Negative regulation of biological process	2.87E-16	Retinoid binding	6.25E-06

development and transcriptional activity while genes in cluster Ect6, with downward trajectories, associated with the negative regulation of biological, cellular processes and retinoid binding, supporting the decreasing reception of RA observed over time in the distal limb bud.

In summary, the temporal transcriptomes of the distal limb bud ectoderm revealed two separate aspects. First a progressive epidermal differentiation trend and second, a peak of signaling activity at E10.5. These two aspects probably reflect the mixture of surface ectoderm and the specialized AER in our samples. Indeed, scRNAseq of the autopod of stage HH25 chick wing buds distinguished two subclusters of "skin" cells one corresponding to the surface skin and the other to the AER.[23] All AER-*Fgfs* showed a maximal expression at E10.5, with *Fgf8*, *Fgf4*, and *Fgf17*, included in cluster Ect3, and *Fgf9* in cluster Ect2, since despite peaking at E10.5, it was still maintained at subsequent stages. The decay in RA-

responsive genes, on the one hand, concomitant with the raise of AER-*Fgfs* signaling, is consistent with the previously proposed mutual antagonism between RA signaling and AER-Fgf expression.[54]

The *Fgf* peak of expression in the ectoderm fits nicely with the peak of mesodermal expression of *Dusp6* and *Spry2* (Mes6), the best-known readouts of Fgf signaling,[74,75] suggesting that not only *Fgf* transcription but also Fgf signaling peaks at E10.5 (see also Figure 7C). Interestingly, a similar decay in *Dusp6* and *Spry2* expression from HH24 (equivalent to E10.5) onwards was also observed in chick (Pickering et al. 2018). In this regard, it is interesting to consider that limb bud development is controlled by a self-regulatory Shh/Gremlin1/Fgf positive feedback signaling system.[76] It was proposed that the termination of limb outgrowth depends on the progressive increase in the level of AER-Fgfs that are able to repress *Grem1* in a dose-dependent manner[77] eventually leading to the breakdown of the Shh-Grem1-Fgf loop. However, this proposal cannot be easily reconciled with our data showing that AER-Fgf expression and signaling peaks at E10.5 that is, well before limb patterning terminates. Our data may instead favour the recently proposed intrinsic progressive increase in BMP signaling described in chick.[46] This intrinsic activation of BMPs is possibly mediated by *Hoxa13*, as Hoxa13 can bind to regulatory regions of *Bmp2* and *Bmp7* and activate the expression of these genes.[78]

Finally, our results clearly show that the transcriptome of the ectoderm is not equivalent across stages. Because of the mixing of surface ectoderm (dorsal and ventral most region) and AER cells in our samples, we can envisage that part of the ectoderm transcriptional changes corresponds to the epidermal differentiation and part to the specific activity of the AER. Even considering only the expression of AER signaling factors, our data does not support a functional equivalence between stages as has been shown by heterochronic recombination experiments in chick. A parsimonious explanation for this discrepancy is that the functional equivalence of the AERs of different stages relies on the AER ability to immediately respond to the mesoderm influence as previously suggested.[6] In this view, the limb progenitors would not only maintain the AER but exert an instructive effect on it by directing its transcriptomic profile and contributing to the intimate connection between the two limb components.

2.8 | Major transcriptional shift between E9.5 and E10.5

The profiles of clusters Mes1, Mes2, Mes5, and Mes6 (Figure 3C) and Ect2, Ect3, and Ect4 (Figure 5C) showed a pronounced change in expression level between E9.5 and E10.5, indicating a major transition in transcriptional regulation occurring between these two stages in the distal limb bud. This is in line with the marked separation between E9.5 and E10.5 samples observed in the PCA plots (Figures 3A and 5A). Furthermore, when comparing between successive stages, the number of DEG in the E9.5 vs E10.5 was substantially larger than in the other comparisons (Figure 6A).

We interpreted the transcriptional shift between E9.5 and E10.5 as reflecting a change from an early transcriptional profile that is mostly a continuation of trunk progenitors and that includes expression of a battery of 3′ *Hox* genes,[57] to a later limb specific transcriptional signature characterized by the starting of the second phase of *Hox* gene expression including *Hoxa13* and *Hoxd13*. This key transcriptional inflection point fits with the switch from an early phase of PD patterning specifying the stylopod that relies on signaling[9,10] to a second phase in which more distal positional values are progressively specified in an intrinsically timed manner possible mediated by the loss of Meis proteins.[6,7] Overall, our results support a relevant role for *Hox* genes as modulators of PD patterning in limb development. Interestingly, the analysis of the temporal transcriptome of the limb bud at single cell resolution also concluded that the transition from an early to a late signature largely relied on the progression of the *HoxA* and *HoxD* clusters.[79]

2.9 | The developmental program of the limb bud ectoderm

To learn more about the transcriptional dynamics over time in the ectodermal limb component, we assessed the number of genes enriched in each tissue layer at any given developmental stage. We found 3452 genes significantly enriched in at least one stage (P-adj < .05 and log2FC > 1.5), 1487 in the mesoderm and 1899 in the ectoderm layer, with 67 genes enriched in both the ectoderm and the mesoderm at different developmental stages ("Summary_MESECT_eachstage.xlsx" in Additional files).

We focused on the 617 genes that were significantly enriched in the ectoderm at all stages, thus potentially including essential ectodermal regulators (Figure 6B). We reasoned that some of these genes would vary in their expression levels over time, reflecting the implementation of an ectoderm developmental program, whereas those remaining constant may instead indicate a more basic involvement into ectodermal structure and function. We identified 366 genes with significant

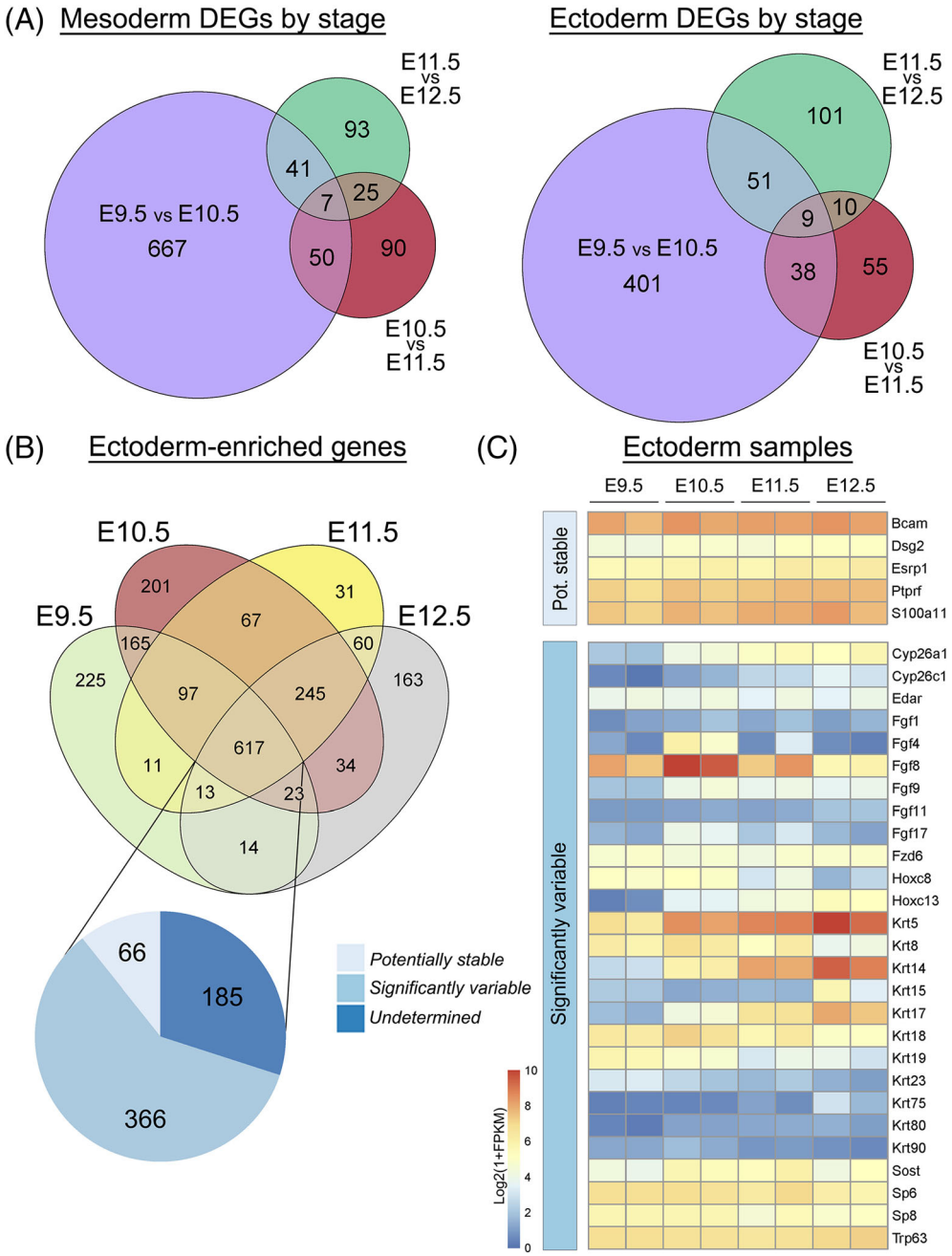

FIGURE 6 Transcriptional shift and ectoderm developmental program. (A) Euler diagrams showing the overlap of the mesodermal differentially expressed genes (DEGs) that varied by stage with *P*-adj < .05 and log2FC > 1.5 after Wald test for the indicated stages of mesoderm (left) or ectoderm (right) samples. Number of genes is indicated for each comparison. Note the larger number of DEGs in the E9.5 vs E10.5 contrast compared with the other contrasts. (B) Venn diagram showing the overlap of the ectoderm-enriched genes obtained by comparing ectoderm and mesoderm at each stage (*P*-adj < .05 and log2FC > 1.5 after Wald test). The 617 genes enriched in the ectoderm in all stage comparisons were considered the ectodermal development program. Based on their *P* values from the LRT test along stages, these 617 genes were further classified as significantly variable genes (366 genes; *P*-adj < .05), potentially stable genes (66 genes; *P* value >0.5) and undetermined (185 genes; *P* value <0.5) as indicated in the pie chart. (C) heatmaps of log2 (1 + FPKM) of representative potentially stable (top) and significantly variable (bottom) genes

variations of their transcript levels (*P*-adj < .05) ("ECT_Signature_Variable.xlsx" in Additional files) and 66 genes displaying no obvious variation (*P* value >.5) ("ECT_Signature_Stable.xlsx" in Additional files). Another set of 185 genes were labeled as undetermined (Figure 6B) ("ECT_Signature_undetermined.xlsx" in Additional files). The list of 66 stable genes expectedly included several genes coding for structural components in basement membranes, epithelial cell-cell junctions and epithelium architecture (ie, *Bcan*, *Dsg2*; Figure 6C). Of note, the *Esrp1* was present in this list, an epithelial specific splicing regulator of the ectoderm specific isoform of *Fgfr2* (*Fgfr2-IIIb*) (Figure 6C).

The list of 366 variable genes included genes involved in the progressive differentiation of the ectoderm and displaying specific temporal patterns of transcription. For instance, it included a wide set of epidermal keratins (*Krt 5, 8, 14, 15, 17, 18, 19, 23, 75, 80, 90*) involved in the epidermal keratinocyte differentiation program to form the mature epidermis, a process that involves keratin modulation and TP63 expression (Figure 6C). Genes involved in the differentiation of the hair and other epidermal derivatives, such as several *Hoxc* members and *Edar*, were also present in this list, which also contained all AER-*Fgfs* as well as the Sp8 and Sp6 transcription factors that

mediate *Wnt*-dependent *Fgf* induction and several modulators of *Wnt* signaling such as *Fzd6* and *Sost*.

2.10 | Signaling pathway analysis during limb bud development

Limb development relies on the continuous crosstalk between the ectoderm and the mesoderm and hence the parallel trajectories followed by the transcriptomes of both limb components may reflect these dynamic interactions. In order to identify pathways preferentially used in the ectoderm or in the mesoderm, we used the Signaling Pathway Impact Analysis (SPIA) package in R.[80] This package extracts over-represented signaling pathways based on a set of differentially expressed genes and the topology of the pathway. As input, we used the DEGs between ectoderm and mesoderm at each stage. SPIA will highlight pathways which are preferentially used in ECT or preferentially used in MES. The results can be visualized in the volcano plots in Figure 7A and in "SPIA_raw_results.xlsx" (Additional files).

The Wnt and Hippo pathways were significantly enriched in the ectoderm at all stages analyzed (*P*GFWER value <.05) whereas the Ras and the MAPK pathways were enriched in one layer or another depending on the stage. These pathways were therefore considered for further study (Figure 7A). Based on their expression profiles and published information, we manually curated the list of most relevant components in each pathway, which were then visualized in heatmaps (Figure 7B-E). We also considered and marked which components of the pathways displayed significant enrichment in transcript level between the two tissue layers at each of the four time points analyzed. It is worth noting here that the BMP pathway, key in limb development, was not included in our study because it did not show any inter-layer enrichment.

The Wnt/β-catenin signaling pathway plays crucial functions in limb bud initiation, outgrowth, early patterning and subsequent morphogenesis in both the mesoderm and ectoderm compartments. In the limb bud ectoderm, it is initially required for AER induction, then for its maintenance.[81,82] Accordingly, the majority of *Wnt* ligands, several of the frizzled receptors (*Fzd1*, *Fzd6*, and *Fzd8*) and a set of associated regulators including *Dkk1*, *Notum*, *Wif1*, *Sost*, *Lgr6*, *Rspo2*, and the E3 ligases *Rnf43* and *Znfr3*, were significantly enriched in the ectoderm (Figure 7B). We noticed the restricted expression of *Sost*, an inhibitor of *Bmp* and *Wnt* signaling, to the non-AER ectoderm (Figure 7B).[83] In contrast, the expression of *Notum*, a Wnt negative feedback regulator, was specifically restricted to the AER with expression peak at E10.5 as visualized in the heatmap and the temporal expression plot (Figure 7B). This analysis supports the predominance of ectodermal *Wnt* signaling during limb development and underscores fine differences in modulation between the AER and the surface ectoderm.

The MAPK pathways are activated by receptor tyrosine kinases, amongst them the FGF receptors.[84] During limb development, AER signaling is mediated by FGFs acting through the RAS/MAP kinase transduction cascade.[85,86] The heatmap of the RAS/MAPK kinase pathway components clearly reflected the expression distribution of *Fgf* ligands and receptors, with a robust enrichment of *Fgf10* and *Fgf2* in the mesoderm and of the AER-*Fgfs* in the ectoderm (Figure 7C). Amongst the *Fgf* receptors, *Fgfr2* was significantly enriched in the ectoderm at all stages, whereas *Fgfr1* appeared slightly upregulated in the mesoderm. The heatmap showed the previously observed peak of expression of the AER-*Fgfs* at E10.5. The gene coding for the dual specificity protein phosphatase Dusp6, that specifically binds to and inactivates ERK1/2 thus acting as Fgf inducible negative regulator of the activity of MAPK, was highly expressed in both the ectoderm and mesoderm cells, suggesting reception of the signal in both layers. As previously mentioned, in the mesoderm, *Dusp6* and *Spry2* had their maximal transcript levels at E10.5, coincident with the peak of AER Fgfs thus reflecting the transmission of the signal from the ectoderm to the mesoderm. We also observed a previously unnoticed yet significant enrichment of *Fgf3* and *Fgf15/19* in the ectoderm (Figure 7C). Of note, *Fgf15/19* has been reported to be expressed in the chick AER, but not in the mouse.[87] Despite WMISH failing to clearly detect *Fgf3* and *Fgf15/19* mRNAs in the limb bud ectoderm, ISH to tissue sections detected the *Fgf3* low level of expression (Figure 7C). These results add two more Fgfs to the set of AER-Fgfs,[16] whose functional impact on AER function remain to be assessed.

The platelet derived growth factor (Pdgf) signaling pathway consists of four ligands (Pdgfa, Pdgfb, Pdgfc, and Pdgfd) and two tyrosine kinase receptors (Pdgfra and Pdgfb).[88] During embryonic development, this signaling system predominantly uses the PI3/AKT transduction pathway and regulates many biological processes including angiogenesis, cell proliferation and differentiation.[85] In our datasets, *Pdgfa* expression showed high transcript levels restricted to the ectoderm, while *Pdgfc* was expressed in both layers although with higher levels in the ectoderm. The other two ligands, *Pdgfb* and *Pdgfd*, showed very low expression levels in both layers (Figure 7D). In addition, the *Pdgfra* and *Pdgfrb* receptors were also expressed in both layers with different enrichment, while *Pdgfrb* showed enrichment in the mesoderm throughout the period studied, the enrichment of *Pdgfra*

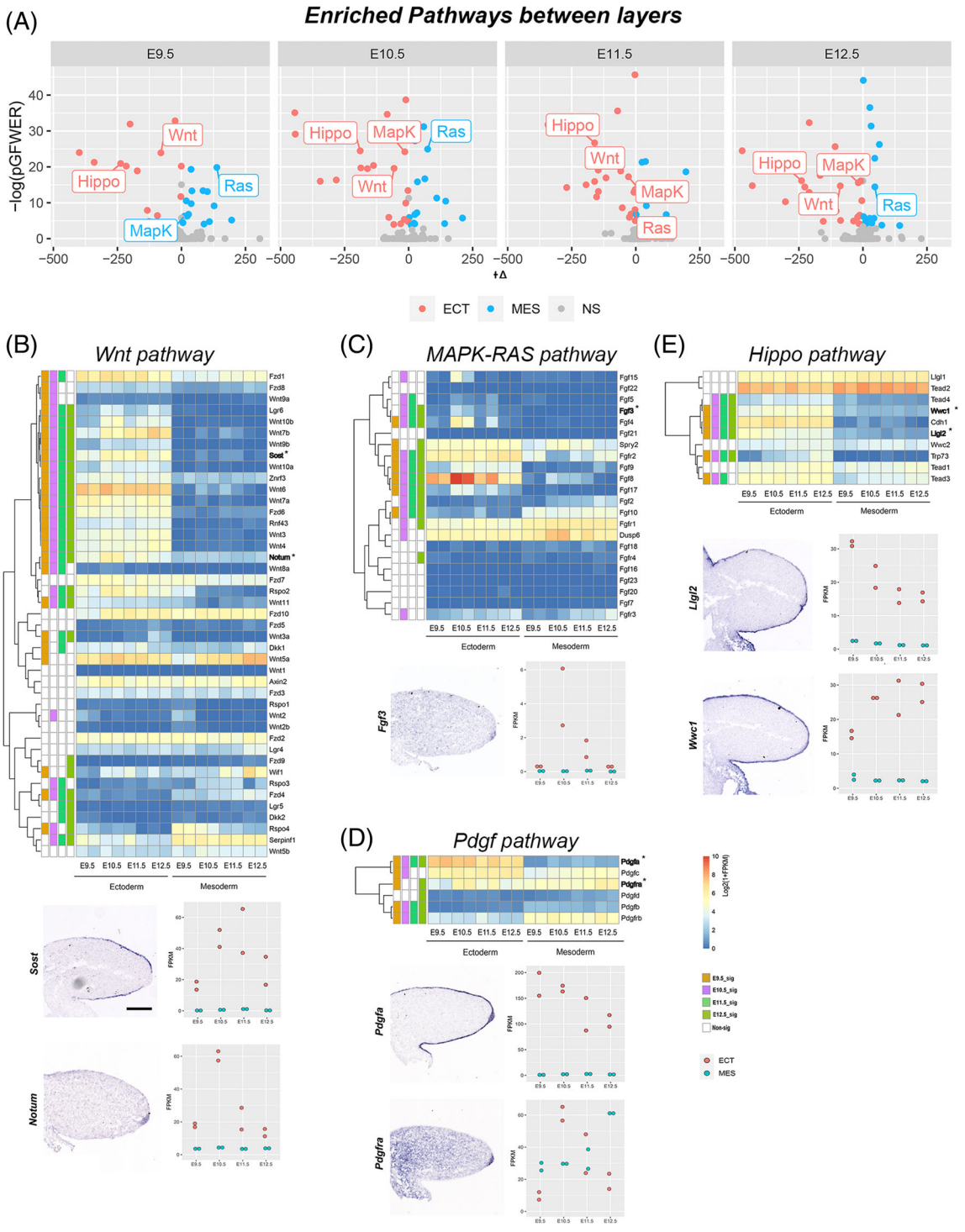

FIGURE 7 Selected signaling pathways with enrichment between ectoderm and mesoderm layers. (A) Volcano plots summarizing the SPIA results in each stage. On the x-axis is tA (observed total accumulation) which indicates if the pathway is significantly more used in ectoderm (*P*GFWER <.05 and tA < 0, red dot) or in mesoderm (*P*GFWER <.05 and tA > 0, blue dot). Grey dots denote non-significant pathways. On the y-axis is the *P* value with Bonferroni correction. The name of the selected pathways is included. (B) Manually curated heatmap of the Wnt pathway (top) and ISH expression pattern and plotted expression profile of *Sost* and *Notum* (bottom). (C) Manually curated heatmap of the Ras-MAPK pathway. Note the peak of expression of AER-Fgfs in the E10.5 ectoderm. The expression pattern and expression profile for *Fgf3* is also shown. (D) Heatmap of the Pdgf pathway components and expression pattern and profile of *Pdgfa* and *Pdgfra*. (E) Heatmap of the Hippo pathway components and expression patterns and temporal profiles of *Llgl2* and *Wwc1*. Heatmaps with log2(1 + FPKM) values include the expression of selected genes in both mesoderm and ectoderm tissues. Colors on the left indicate a significant enrichment of log2FC >1.5 of a gene in mesoderm or ectoderm at this stage (*P*-adj < .05 and log2FC > 1.5). All ISH show longitudinal sections E10.5 forelimb buds. Scale bar is 150 μm

was stage dependent. *In situ* detection experiments in both whole mount and tissue sections validated these results (Figure 7D). Activation of the Pdgf pathway across adjacent layers has already been noted in different embryonic contexts.[89] In most cases the receptor was expressed in the mesenchyme, whereas the ligand was in the epithelium, as we observed in the developing limb. The function of this pathway during limb development nevertheless remains elusive.

We finally looked at the Hippo signaling pathway, which is highly conserved between invertebrates and vertebrates and involved in the growth response to mechanical forces.[90-93] While several studies have shown the role of the Hippo pathway during skeletal development, its function during early stages of limb development has received less attention. Here we show that many of its core components including *Wwc1*, *Llgl2*, *Tead3*, *Tead4*, and *Trp73* were robustly expressed and significantly enriched in the ectoderm compartment, an observation confirmed by ISH experiments (Figure 7E), which may be relevant since the upregulation of both *Wwc1* and *Llgl2* prevents YAP/TAZ from entering the nucleus and thus the activation of the signaling cascade. During facial development, it was suggested that this pathway coordinates growth of the overlying ectoderm in response to the mesoderm growth, by sensing the ectoderm tension.[94] Our observation suggest that a similar mechanism may be at work in the growing limb.

3 | CONCLUSIONS

The temporal transcriptomes of the distal limb progenitors that we have generated in this study provide a valuable genomic resource, which contains relevant temporal and spatial information that may help refine our current understanding of limb development, in particular regarding the progression of PD patterning. Our datasets are also very valuable for examining alternative splicing and isoforms between the ectoderm and mesoderm in the developing distal limb bud.

Our comprehensive analysis of the expression profile of the population of distal limb progenitors shows that they progressively lose their stemness state in association with an increase in skeletal specification. This is noteworthy, considering the frequent assumption that distal mesoderm cells remain undifferentiated as long as they are under the influence of the AER.

The transcriptome of early (E9.5) limb progenitors appears as a continuation of that observed in trunk progenitors from which they derive and include also stylopod-associated markers, RA responsive genes and 3′ *Hox* genes of all clusters. The profile of late distal limb progenitors, instead, is characterized by the skeletal differentiation and expression of 5′ *Hox* genes. This progression towards differentiation with developmental time correlates with the stepwise implementation of *Hox* clusters.

The time-sequenced transcriptomes of the distal limb bud ectoderm reveal a mixture of the progressive epidermal differentiation of the surface ectoderm, on the one hand, and the specialized activity of the AER cells, on the other hand. We show that the peak of AER FGF activity occurs at E10.5, that is, likely too early to explain the termination of the Shh-Grem1-Fgf autoregulatory loop. Considering only the temporal changes attributed to the AER, our data does not support a functional equivalence of the AER throughout limb development, as concluded from heterochronic recombination experiments in chick. In contrast, we propose that the functional equivalence of the AER along limb development relies on its ability to rapidly respond and adapt to the mesoderm influence as previously suggested. In this view, the limb progenitors would not only maintain the AER but also exert an instructive effect by impacting its transcriptomic profile and contributing to the intimate and necessary connection between the two limb components.

The analysis of such interactions between the mesoderm and ectoderm is complicated by the fact that the same signaling pathways are used either between layers, or within each layer. The SPIA analysis allowed to identify signaling pathways differentially enriched between layers and revealed the preferential expression of Hippo pathway components in the ectoderm.

4 | EXPERIMENTAL PROCEDURES

4.1 | Mouse embryos

Embryos from the mouse inbred line C57BL/6J were used. Noon of the day of the vaginal plug was defined as Embryonic day (E) 0.5. Embryos of the desired developmental stage were collected, dissected in Phosphate Buffered Saline (PBS) and processed as required. All animal procedures were either conducted accordingly to the EU regulations and 3R principles and reviewed and approved by the Bioethics Committee of the University of Cantabria, or performed in accordance with the Swiss Animal Welfare Act (LPA), under the license no. GE 81/14 (to DD).

4.2 | Preparation of samples for RNA-seq, ectoderm-mesoderm separation

Forelimbs of embryos of the desired stage were collected in ice-cold PBS and distal bands of 150 μm were carefully

dissected (Figure 1A). Then, to separate the ectoderm and the mesoderm components, the dissected bands of distal tissue were subject to mild digestion in 0.25% trypsin (HyClone Trypsin Protease, SV30037.01) on ice. After a quick wash in cold PBS + 10% FBS, the separation of the two limb components was completed in cold PBS with the help of fine forceps. For each replicate, the mesoderm and ectoderm samples came from the same pool of approximately 25 limb buds.

4.3 | RNA sequencing

Two biological replicates were prepared from two independent pools of forelimb buds of each of the stages analyzed (E9.5, E10.5, E11.5, and E12.5) for both mesoderm and ectoderm. Total RNAs were purified using the RNeasy Mini Kit (QIAGEN, Cat No./ID: 74104) or the RNeasy Plus Mini Kit (QIAGEN, Cat No./ID: 74134). RNA libraries were prepared using the Truseq Stranded mRNA Library Prep kit (Illumina, Cat No./ID: 20020594) and 100-bp single-end reads were generated.

The gtf from ensembl version 93 was filtered to remove read through transcripts and all noncoding transcripts (retained-intron, nonsense-mediated decay, etc.) from a protein-coding gene. In addition, all genes with the same gene name which overlaps were merged under the same gene to avoid ambiguous reads. Adapters and bad-quality bases were removed with Cutadapt version 1.16 options -m 15 -a GATCGGAAGAGCACACGTCTGAACTCCAGTCAC -q 30. Reads were further mapped using STAR version 2.6.0c with ENCODE parameters with the gtf file described above. FPKM values were computed with cufflinks version 2.2.1 omitting mitochondrial genes. These transcriptomic datasets were initially reported and validated in Reference 26.

4.4 | Statistical analyses

Only protein coding genes were considered in this study. All statistical analyses and plots were performed using custom scripts in R version 4.0.3 (www.r-project.org). Differential gene expression analyses were performed using the DESeq2 R Bioconductor package.[95] For pairwise comparations, the Wald test was used and in those comparations including all embryonic stages, the Likelihood Ratio Test (LRT) was used to evaluate the gene expression changes across different conditions, with a threshold of significance of adjusted P value = .05.

For Principal Component Analysis (PCA) only the 500 protein coding genes with the higher variance were considered, using log2(1 + FPKM) values. To study reduced sets of differentially expressed genes, heatmaps with log2(1 + FPKM) values were generated. To display the differentially expressed genes across the mesoderm samples (MES-DEGs) or the ectoderm samples (ECT-DEGs), FPKM values were renormalized on the basis of rank-conserved genes and a median-scaling procedure using the 1000 genes with the least expression rank variation across samples.[96] Clustered heatmaps were generated using Pearson correlation coefficient as distance, with centered and scaled log2(1 + FPKM) values. The clustering was cut to separate MES-DEGs in seven clusters and ECT-DEGs in six clusters. A line chart was performed with the mean of the values on the heatmap for a given cluster for each time point. Gene Ontology (GO) enrichment analyses were performed using the goseq R Bioconductor package[97] to identify statistically overrepresented terms in GO Biological Process (GO:BP) and Molecular Function (GO:MF) categories (the 20 most enriched GO terms for each category are available in Additional files under the name "Global_PC1_and_PC2_Enriched_GO_terms.xlsx" and "MES_and_ECT_clusters_Enriched_GO_terms.xlsx").

To study alternative splicing, exon coverage was evaluated with DEXseq version 1.38.0[28] on uniquely mapped reads (see https://github.com/lldelisle/scriptsForFernandezGuerreroEtAl2020). Gene aggregation was disabled to better estimate the relative exon usage on each gene. Only exons belonging to protein coding genes were kept and DEXseq analysis was run with default parameters comparing the eight samples of mesoderm to the eight samples of ectoderm. Exonic parts were considered as differentially used in one tissue layer when adjusted P value <.05. The coverage plot in Figure 2C was generated using pyGenomeTracks.[98,99] To obtain the genes enriched in one of the two tissues (ectoderm or mesoderm) at each time point, a Wald test of ectoderm vs mesoderm samples was performed and significant genes (P-adj < .05 and log2FC > 1.5) that were extracted. 3452 genes were significantly enriched in one of the tissues at least in one stage. From these, 1487 were enriched in the mesoderm, and 1899 in the ectoderm. From the ectoderm enriched genes, the 617 genes that were enriched at all stages were extracted. A Venn diagram to depict intersections between ectoderm-enriched genes was obtained with R package eulerr. An LRT test on this subset was performed to obtain DEGs across stages and resulting P values were used to separate the 617 genes in three groups: Genes with P value >.5 were treated as potentially stable genes (66), genes with P-adjusted value <.05 were treated as significantly variable genes (366), and the remaining genes were labeled as undetermined genes. A pie chart of the distribution of the ectoderm developmental program genes was plotted with ggplot2 R package.

For the pathway enrichment analysis we used the SPIA R package.[80] At each stage, the log2FC of ectoderm- or mesoderm-enriched genes (see above) were used as input. Pathways that were significant (*P*GFWER value <.05 [Bonferroni correction] and tA < or > 0 for ECT and MES, respectively) at all stages analyzed were considered for further studies. Then, expression heatmaps were constructed with genes that, based on previous published information and their expression values and statistical significance, were considered most relevant.

4.5 | *In situ* hybridization

Embryos were dissected out in ice-cold PBS and fixed overnight (ON) in 4% paraformaldehyde (PFA) in PBS and embedded in paraffin or stored in 100% methanol. For WMISH, embryo permeabilization was performed with proteinase K (10 μg/ml) at room temperature for a variable time depending on the stage of the embryo to study mesodermal expressions and with a lower concentration of proteinase K (5 μg/ml) for 5 min to study ectodermal expressions. For *in situ* hybridization on paraffin sections permeabilization was performed by incubation in PK (10 μg/ml) for 7.5 min at room temperature. Sections were post-fixed with 4% PFA, followed by an acetylation step to reduce background signal. Both in whole mount and in tissue sections, hybridization was performed using in vitro transcribed digoxigenin-labelled antisense RNA probes, at 65°C ON. After washing, embryos or tissue sections were incubated with alkaline phosphatase-conjugated anti-digoxigenin antibody (Roche, 16 646 821) ON at 4°C and detection reactions were performed with NBT (Promega, S3771)/BCIP (Roche, 16 853 423). Primers used to amplify cDNA templates for riboprobe synthesis are included in Table 3. A minimum of three forelimbs were used for each probe and stage.

TABLE 3 Primers used to amplify cDNA templates for riboprobe synthesis

Primer name	Sequence (5′-3′)
Mouse *Hoxb6*	Fwd: GAGGAGGAGGAGGAAAAGCC Rev: GGGGACATGGACGAAATGAG
Mouse *Llgl2*	Fwd: CAATTGGCATCCTCACCGC Rev: AGTGAAGACGAAACAAGGTGT
Mouse *Rprm*	Fwd: ACCGGAGGCCGTCTAAAG Rev: GGGCGTAAACCGTGCAGAC
Mouse *Notum*	Fwd: CAGGGCAAGAGATGAACGTG Rev: AACAGATACGGGGTGGGAAG
Mouse *Tle3*	Fwd: TTCCGTTTCTCCCACAGACA Rev: CGGCTCCCCAACTCTCTTAT
Mouse *Wwc1*	Fwd: AGTGCAGTCTTTCAGGGAGA Rev: ACAGTTTTAAGACTAGCAGCCAC

ACKNOWLEDGMENTS

This manuscript is dedicated to the memory of Professor John F. Fallon, a brilliant scientist, revered mentor and enthusiastic colleague whose more than 40 years of research contributed in fundamental ways to our understanding of limb development. We thank Laura Galán for excellent technical assistance. This study was supported by funds from the Ecole Polytechnique Fédérale (EPFL, Lausanne), the University of Geneva and the Swiss National Research Fund (No. 310030B_138662) to Denis Duboule and by the Spanish Ministry of Science, Innovation and Universities Grant BFU2017-88265-P to Marian Ros. Sofía Zdral was supported by a Ph.D. fellowship from the University of Cantabria. Lucille Lopez-Delisle was supported by the ERC Grant RegulHox (No. 588029, to Denis Duboule).

AUTHOR CONTRIBUTIONS

Marc Fernandez-Guerrero: Data curation; formal analysis; investigation; methodology; validation; visualization; writing-review & editing. **Sofía Zdral:** Data curation; formal analysis; investigation; methodology; validation; visualization; writing-review & editing. **Alejandro Castilla-Ibeas:** Data curation; formal analysis; investigation; methodology; validation; visualization; writing-review & editing. **Lucille Lopez-Delisle:** Data curation; formal analysis; investigation; methodology; resources; software; supervision; validation; visualization; writing-review & editing.

DATA AVAILABILITY STATEMENT

All raw and processed datasets of RNA-seq are available in the Gene Expression Omnibus (GEO) repository (accession no. GSE150702). The bioinformatics scripts needed to reproduce the figures and tables from raw data and the additional files (gene lists with FPKMs and top 20 enriched GOs for each comparation) have been deposited at GitHub, https://github.com/lldelisle/scriptsForFernandezGuerreroEtAl2021.

ORCID

Denis Duboule https://orcid.org/0000-0001-9961-2960
Marian A. Ros https://orcid.org/0000-0002-1224-7671

REFERENCES

1. Fernandez-Teran M, Ros MA. The apical ectodermal ridge: morphological aspects and signaling pathways. *Int J Dev Biol*. 2008;52(7):857-871. https://doi.org/10.1387/ijdb.072416mf
2. Saunders JW. The proximo-distal sequence of origin of the parts of the chick wing and the role of the ectoderm. *J Exp*

Zool. 1948;108(3):363-404. https://doi.org/10.1002/jez.1401080304
3. Rowe DA, Cairns JM, Fallon JF. Spatial and temporal patterns of cell death in limb bud mesoderm after apical ectodermal ridge removal. *Dev Biol*. 1982;93(1):83-91. https://doi.org/10.1016/0012-1606(82)90241-X
4. Summerbell D, Lewis JH, Wolpert L. Positional information in Chick limb morphogenesis. *Nature*. 1973;244:492-496. https://doi.org/10.1038/244492a0
5. Tabin C, Wolpert L. Rethinking the proximodistal axis of the vertebrate limb in the molecular era. *Genes Dev*. 2007;21(12):1433-1442. https://doi.org/10.1101/gad.1547407
6. Saiz-Lopez P, Chinnaiya K, Campa VM, Delgado I, Ros MA, Towers M. An intrinsic timer specifies distal structures of the vertebrate limb. *Nat Commun*. 2015;6(8108):1-9. https://doi.org/10.1038/ncomms9108
7. Delgado I, López-Delgado AC, Alberto RD, et al. Proximodistal positional information encoded by an Fgf-regulated gradient of homeodomain transcription factors in the vertebrate limb. *Sci Adv*. 2020;6(23):eaaz0742. https://doi.org/10.1126/sciadv.aaz0742
8. McQueen C, Towers M. Establishing the pattern of the vertebrate limb. *Development*. 2020;147(17):dev177956. https://doi.org/10.1242/dev.177956
9. Cooper KL, Cooper KL, Hu JK, et al. Initiation of proximal-distal patterning in the vertebrate limb by signals and growth. *Science (80-)*. 2011;332(6033):1083-1087. https://doi.org/10.1126/science.1199499
10. Rosello-Diez A, Ros MA, Torres M. Diffusible signals, not autonomous mechanisms, determine the main proximodistal limb subdivision. *Science (80-)*. 2011;332(6033):1086-1088. https://doi.org/10.1126/science.1199489
11. Tarchini B, Duboule D. Control of Hoxd genes' collinearity during early limb development. *Dev Cell*. 2006;10(1):93-103. https://doi.org/10.1016/j.devcel.2005.11.014
12. Rubin L, Saunders JW. Ectodermal-mesodermal interactions in the growth of limb buds in the chick embryo: Constancy and temporal limits of the ectodermal induction. *Dev Biol*. 1972;28(1):94-112. https://doi.org/10.1016/0012-1606(72)90129-7
13. Zwilling E. Interaction between ectoderm and mesoderm in duck-chicken limb bud chimaeras. *J Exp Zool*. 1959;142:521-532. https://doi.org/10.1002/jez.140142012
14. Fernandez-Teran M, Piedra ME, Ros MA, Fallon JF. The recombinant limb as a model for the study of limb patterning, and its application to muscle development. *Cell Tissue Res*. 1999;296(1):121-129. https://doi.org/10.1007/s004410051273
15. Kuhlman J, Niswander L. Limb deformity proteins: role in mesodermal induction of the apical ectodermal ridge. *Development*. 1997;124(1):133-139.
16. Mariani FV, Ahn CP, Martin GR. Genetic evidence that FGFs have an instructive role in limb proximal-distal patterning. *Nature*. 2008;453(7193):401-405. https://doi.org/10.1038/nature06876
17. Vargesson N, Clarke JDW, Vincent K, Coles C, Wolpert L, Tickle C. Cell fate in the chick limb bud and relationship to gene expression. *Development*. 1997;124:1909-1918.
18. Sato K, Koizumi Y, Takahashi M, Kuroiwa A, Tamura K. Specification of cell fate along the proximal-distal axis in the developing chick limb bud. *Development*. 2007;134(7):1397-1406. https://doi.org/10.1242/dev.02822
19. Reinhardt R, Gullotta F, Nusspaumer G, et al. Molecular signatures identify immature mesenchymal progenitors in early mouse limb buds that respond differentially to morphogen signaling. *Dev*. 2019;146(10):dev173328. https://doi.org/10.1242/dev.173328
20. Beccari L, Yakushiji-Kaminatsui N, Woltering JM, et al. A role for HOX13 proteins in the regulatory switch between TADs at the HoxD locus. *Genes Dev*. 2016;30(10):1172-1186. https://doi.org/10.1101/gad.281055.116
21. Sheth R, Barozzi I, Langlais D, et al. Distal limb patterning requires modulation of cis-regulatory activities by HOX13. *Cell Rep*. 2016;17(11):2913-2926. https://doi.org/10.1016/j.celrep.2016.11.039
22. Cao J, Spielmann M, Qiu X, et al. The single-cell transcriptional landscape of mammalian organogenesis. *Nature*. 2019;566(7745):496-502. https://doi.org/10.1038/s41586-019-0969-x
23. Feregrino C, Sacher F, Parnas O, Tschopp P. A single-cell transcriptomic atlas of the developing chicken limb. *BMC Genomics*. 2019;20(1):1-15. https://doi.org/10.1186/s12864-019-5802-2
24. Boehm B, Rautschka M, Quintana L, Raspopovic J, Jan Ž, Sharpe J. A landmark-free morphometric staging system for the mouse limb bud. *Development*. 2011;138(6):1227-1234. https://doi.org/10.1242/dev.057547
25. Pizette S, Niswander L. BMPs negatively regulate structure and function of the limb apical ectodermal ridge. *Development*. 1999;126(5):883-894.
26. Fernandez-Guerrero M, Yakushiji-Kaminatsui N, Lopez-Delisle L, et al. Mammalian-specific ectodermal enhancers control the expression of Hoxc genes in developing nails and hair follicles. *Proc Natl Acad Sci USA*. 2020;117(48):30509-30519. https://doi.org/10.1073/pnas.2011078117
27. Wang ET, Sandberg R, Luo S, et al. Alternative isoform regulation in human tissue transcriptomes. *Nature*. 2008;456(7221):470-476. https://doi.org/10.1038/nature07509
28. Anders S, Reyes A, Huber W. Detecting differential usage of exons from RNA-seq data. *Genome Res*. 2012;22(10):2008-2017. https://doi.org/10.1101/gr.133744.111
29. Itoh N. FGF10: A multifunctional mesenchymal-epithelial signaling growth factor in development, health, and disease. *Cytokine Growth Factor Rev*. 2016;28:63-69. https://doi.org/10.1016/j.cytogfr.2015.10.001
30. Efroni S, Duttagupta R, Cheng J, et al. Global transcription in pluripotent embryonic stem cells. *Cell Stem Cell*. 2008;2(5):437-447. https://doi.org/10.1016/j.stem.2008.03.021
31. Dudley AT, Ros MA, Tabin CJ. A re-examination of proximodistal patterning during vertebrate limb development. *Nature*. 2002;418(6897):539-544. https://doi.org/10.1038/nature00945
32. Tsialikas J, Romer-Seibert J. LIN28: roles and regulation in development and beyond. *Development*. 2015;142(14):2397-2404. https://doi.org/10.1242/dev.117580
33. Zhang J, Ratanasirintrawoot S, Chandrasekaran S, et al. LIN28 regulates stem cell metabolism and conversion to primed pluripotency. *Cell Stem Cell*. 2016;19(1):66-80. https://doi.org/10.1016/j.stem.2016.05.009
34. Rao S, Zhen S, Roumiantsev S, McDonald LT, Yuan G-C, Orkin SH. Differential roles of Sall4 isoforms in embryonic stem cell pluripotency. *Mol Cell Biol*. 2010;30(22):5364-5380. https://doi.org/10.1128/mcb.00419-10

35. Buganim Y, Markoulaki S, van Wietmarschen N, et al. The developmental potential of iPSCs is greatly influenced by reprogramming factor selection. *Cell Stem Cell*. 2014;15(3):295-309. https://doi.org/10.1016/j.stem.2014.07.003
36. Akiyama R, Kawakami H, Wong J, Oishi I, Nishinakamura R, Kawakami Y. Sall4-Gli3 system in early limb progenitors is essential for the development of limb skeletal elements. *Proc Natl Acad Sci U S A*. 2015;112(16):5075-5080. https://doi.org/10.1073/pnas.1421949112
37. Fernandez A, Huggins IJ, Perna L, et al. The WNT receptor FZD7 is required for maintenance of the pluripotent state in human embryonic stem cells. *Proc Natl Acad Sci U S A*. 2014;111(4):1409-1414. https://doi.org/10.1073/pnas.1323697111
38. Yokoyama S, Ito Y, Ueno-Kudoh H, et al. A systems approach reveals that the Myogenesis genome network is regulated by the transcriptional repressor RP58. *Dev Cell*. 2009;17(6):836-848. https://doi.org/10.1016/j.devcel.2009.10.011
39. Yokoyama S, Hashimoto M, Shimizu H, et al. Dynamic gene expression of Lin-28 during embryonic development in mouse and chicken. *Gene Expr Patterns*. 2008;8(3):155-160. https://doi.org/10.1016/j.gep.2007.11.001
40. Aires R, de Lemos L, Nóvoa A, et al. Tail bud progenitor activity relies on a network comprising Gdf11, Lin28, and Hox13 genes. *Dev Cell*. 2019;48(3):383-395.e8. doi:https://doi.org/10.1016/j.devcel.2018.12.004
41. Yashiro K, Zhao X, Uehara M, et al. Regulation of retinoic acid distribution is required for proximodistal patterning and outgrowth of the developing mouse limb. *Dev Cell*. 2004;6(3):411-422. https://doi.org/10.1016/S1534-5807(04)00062-0
42. Pennimpede T, Cameron DA, MacLean GA, Petkovich M. Analysis of Cyp26b1/Rarg compound-null mice reveals two genetically separable effects of retinoic acid on limb outgrowth. *Dev Biol*. 2010;339(1):179-186. https://doi.org/10.1016/j.ydbio.2009.12.024
43. Thumkeo D, Watanabe S, Narumiya S. Physiological roles of rho and rho effectors in mammals. *Eur J Cell Biol*. 2013;92(10–11):303-315. https://doi.org/10.1016/j.ejcb.2013.09.002
44. Vicente-Manzanares M, Ma X, Adelstein RS, Horwitz AR. Non-muscle myosin II takes Centre stage in cell adhesion and migration. *Nat Rev Mol Cell Biol*. 2009;10(11):778-790. https://doi.org/10.1038/nrm2786
45. Ohki R, Nemoto J, Murasawa H, et al. Reprimo, a new candidate mediator of the p53-mediated cell cycle arrest at the G2 phase. *J Biol Chem*. 2000;275(30):22627-22630. https://doi.org/10.1074/jbc.C000235200
46. Pickering J, Rich CA, Stainton H, et al. An intrinsic cell cycle timer terminates limb bud outgrowth. *Elife*. 2018;7:e37429. https://doi.org/10.7554/elife.37429
47. Wichmann IA, Zavala K, Hoffmann FG, et al. Evolutionary history of the reprimo tumor suppressor gene family in vertebrates with a description of a new reprimo gene lineage. *Gene*. 2016;592(1):245-254. https://doi.org/10.1016/j.gene.2016.07.036
48. Xu M, Knox AJ, Michaelis KA, et al. Reprimo (RPRM) is a novel tumor suppressor in pituitary tumors and regulates survival, proliferation, and Tumorigenicity. *Endocrinology*. 2012;153(7):2963-2973. https://doi.org/10.1210/en.2011-2021
49. Lopez-Rios J, Speziale D, Robay D, et al. GLI3 constrains digit number by controlling both progenitor proliferation and BMP-dependent exit to Chondrogenesis. *Dev Cell*. 2012;22(4):837-848. https://doi.org/10.1016/j.devcel.2012.01.006
50. ten Berge D, Brugmann SA, Helms JA, Nusse R. Wnt and FGF signals interact to coordinate growth with cell fate specification during limb development. *Development*. 2008;135(19):3247-3257. https://doi.org/10.1242/dev.023176
51. Ravasi T, Suzuki H, Cannistraci CV, et al. An atlas of combinatorial transcriptional regulation in mouse and man. *Cell*. 2010;140:744-752. https://doi.org/10.1016/j.cell.2010.01.044
52. Li D, Sakuma R, Vakili NA, et al. Formation of proximal and anterior limb skeleton requires early function of Irx3 and Irx5 and is negatively regulated by shh signaling. *Dev Cell*. 2014;29(2):233-240. https://doi.org/10.1016/j.devcel.2014.03.001
53. Capdevila J, Tsukui T, Esteban CR, Zappavigna V, Belmonte JCI. Control of vertebrate limb outgrowth by the proximal factor Meis2 and distal antagonism of BMPs by Gremlin. *Mol Cell*. 1999;4(5):839-849. https://doi.org/10.1016/S1097-2765(00)80393-7
54. Mercader N, Leonardo E, Piedra ME, Martínez-A C, Ros MA, Torres M. Opposing RA and FGF signals control proximodistal vertebrate limb development through regulation of Meis genes. *Development*. 2000;127(18):3961-3970. http://www.ncbi.nlm.nih.gov/pubmed/10952894
55. Capellini TD. Pbx1/Pbx2 requirement for distal limb patterning is mediated by the hierarchical control of Hox gene spatial distribution and Shh expression. *Development*. 2006;133(11):2263-2273. https://doi.org/10.1242/dev.02395
56. Capellini TD, Vaccari G, Ferretti E, et al. Scapula development is governed by genetic interactions of Pbx1 with its family members and with Emx2 via their cooperative control of Alx1. *Development*. 2010;137(15):2559-2569. https://doi.org/10.1242/dev.048819
57. Berenguer M, Meyer KF, Yin J, Duester G. Discovery of genes required for body axis and limb formation by global identification of retinoic acid-regulated epigenetic marks. *PLoS Biol*. 2020;18(5):e3000719. https://doi.org/10.1371/journal.pbio.3000719
58. Cobb J, Dierich A, Huss-Garcia Y, Duboule D. A mouse model for human short-stature syndromes identifies Shox2 as an upstream regulator of Runx2 during long-bone development. *Proc Natl Acad Sci U S A*. 2006;103(12):4511-4515. https://doi.org/10.1073/pnas.0510544103
59. Neufeld SJ, Wang F, Cobb J. Genetic interactions between Shox2 and Hox genes during the regional growth and development of the mouse limb. *Genetics*. 2014;198(3):1117-1126. https://doi.org/10.1534/genetics.114.167460
60. Cunningham TJ, Zhao X, Sandell LL, Evans SM, Trainor PA, Duester G. Antagonism between retinoic acid and fibroblast growth factor signaling during limb development. *Cell Rep*. 2013;3(5):1503-1511. https://doi.org/10.1016/j.celrep.2013.03.036
61. Sweetman D, Smith T, Farrell ER, Chantry A, Münsterberg A. The conserved glutamine-rich region of chick Csal1 and Csal3 mediates protein interactions with other Spalt family members: implications for townes-brocks syndrome. *J Biol Chem*. 2003;278(8):6560-6566. https://doi.org/10.1074/jbc.M209066200
62. Kawakami Y, Uchiyama Y, Esteban CR, et al. Sall genes regulate region-specific morphogenesis in the mouse limb by modulating Hox activities. *Development*. 2009;136(4):585-594. https://doi.org/10.1242/dev.027748
63. Nagai T, Aruga J, Minowa O, et al. Zic2 regulates the kinetics of neurulation. *Proc Natl Acad Sci U S A*. 2000;97(4):1618-1623. https://doi.org/10.1073/pnas.97.4.1618

64. Bork P. Hundreds of ankyrin-like repeats in functionally diverse proteins: Mobile modules that cross phyla horizontally? *Proteins Struct Funct Genet*. 1993;17(4):363-374. https://doi.org/10.1002/prot.340170405
65. Sedgwick SG, Smerdon SJ. The ankyrin repeat: A diversity of interactions on a common structural framework. *Trends Biochem Sci*. 1999;24(8):311-316. https://doi.org/10.1016/S0968-0004(99)01426-7
66. Li J, Mahajan A, Tsai MD. Ankyrin repeat: A unique motif mediating protein-protein interactions. *Biochemistry*. 2006;45(51):15168-15178. https://doi.org/10.1021/bi062188q
67. Yokoyama S, Furukawa S, Kitada S, et al. Analysis of transcription factors expressed at the anterior mouse limb bud. *PLoS One*. 2017;12(5):e0175673. https://doi.org/10.1371/journal.pone.0175673
68. Suzuki T, Hasso SM, Fallon JF. Unique SMAD1/5/8 activity at the phalanx-forming region determines digit identity. *Proc Natl Acad Sci U S A*. 2008;105(11):4185-4190. https://doi.org/10.1073/pnas.0707899105
69. Stricker S, Mundlos S. Mechanisms of digit formation: human malformation syndromes tell the story. *Dev Dyn*. 2011;240(5):990-1004. https://doi.org/10.1002/dvdy.22565
70. Li Y, Qiu Q, Watson SS, Schweitzer R, Johnson RL. Uncoupling skeletal and connective tissue patterning: conditional deletion in cartilage progenitors reveals cell-autonomous requirements for Lmx1b in dorsal-ventral limb patterning. *Development*. 2010;137(7):1181-1188. https://doi.org/10.1242/dev.045237
71. Hojo H, Ohba S, He X, Lai LP, McMahon AP. Sp7/Osterix is restricted to bone-forming vertebrates where it acts as a dlx co-factor in osteoblast specification. *Dev Cell*. 2016;37(3):238-253. https://doi.org/10.1016/j.devcel.2016.04.002
72. Ramakrishnan A-B, Sinha A, Fan VB, Cadigan KM. The Wnt transcriptional switch: TLE removal or inactivation? *Bioessays*. 2018;40(2):1700162. https://doi.org/10.1002/bies.201700162
73. Jo A, Denduluri S, Zhang B, et al. The versatile functions of Sox9 in development, stem cells, and human diseases. *Genes Dis*. 2014;1(2):149-161. https://doi.org/10.1016/j.gendis.2014.09.004
74. Chambers D, Mason I. Expression of sprouty2 during early development of the chick embryo is coincident with known sites of FGF signalling. *Mech Dev*. 2000;91(1–2):361-364. https://doi.org/10.1016/S0925-4773(99)00288-9
75. Eblaghie MC, Lunn JS, Dickinson RJ, et al. Negative feedback regulation of FGF signaling levels by Pyst1/MKP3 in Chick embryos. *Curr Biol*. 2003;13(12):1009-1018. https://doi.org/10.1016/s0960-9822(03)00381-6
76. Zuniga A, Zeller R. Dynamic and self-regulatory interactions among gene regulatory networks control vertebrate limb bud morphogenesis. *Curr Top Dev Biol*. 2020;139:61-88. https://doi.org/10.1016/bs.ctdb.2020.02.005
77. Verheyden JM, Sun X. An Fgf/Gremlin inhibitory feedback loop triggers termination of limb bud outgrowth. *Nature*. 2008;454(7204):638-641. https://doi.org/10.1038/nature07085
78. Knosp WM, Scott V, Bächinger HP, Stadler HS. HOXA13 regulates the expression of bone morphogenetic proteins 2 and 7 to control distal limb morphogenesis. *Development*. 2004;131(18):4581-4592. https://doi.org/10.1242/dev.01327
79. Desanlis I, Kherdjemil Y, Mayran A, et al. HOX13-dependent chromatin accessibility underlies the transition towards the digit development program. *Nat Commun*. 2020;11:2491. https://doi.org/10.1038/s41467-020-16317-2
80. Tarca AL, Draghici S, Khatri P, et al. A novel signaling pathway impact analysis. *Bioinformatics*. 2009;25(1):75-82. https://doi.org/10.1093/bioinformatics/btn577
81. Soshnikova N, Zechner D, Huelsken J, et al. Genetic interaction between Wnt/beta-catenin and BMP receptor signaling during formation of the AER and the dorsal-ventral axis in the limb. *Genes Dev*. 2003;17(16):1963-1968. https://doi.org/10.1101/gad.263003
82. Barrow JR, Thomas KR, Boussadia-Zahui O, et al. Ectodermal Wnt3/beta-catenin signaling is required for the establishment and maintenance of the apical ectodermal ridge. *Genes Dev*. 2003;17(3):394-409. https://doi.org/10.1101/gad.1044903
83. Collette NM, Yee CS, Murugesh D, et al. Sost and its paralog Sostdc1 coordinate digit number in a Gli3-dependent manner. *Dev Biol*. 2013;383(1):90-105. https://doi.org/10.1016/j.ydbio.2013.08.015
84. Mason JM, Morrison DJ, Basson MA, Licht JD. Sprouty proteins: multifaceted negative-feedback regulators of receptor tyrosine kinase signaling. *Trends Cell Biol*. 2006;16(1):45-54. https://doi.org/10.1016/j.tcb.2005.11.004
85. Vasudevan HN, Mazot P, He F, Soriano P. Receptor tyrosine kinases modulate distinct transcriptional programs by differential usage of intracellular pathways. *Elife*. 2015;4:e07186. https://doi.org/10.7554/eLife.07186
86. Smith TG, Karlsson M, Lunn JS, et al. Negative feedback predominates over cross-regulation to control ERK MAPK activity in response to FGF signalling in embryos. *FEBS Lett*. 2006;580(17):4242-4245. https://doi.org/10.1016/j.febslet.2006.06.081
87. Kurose H, Bito T, Adachi T, Shimizu M, Noji S, Ohuchi H. Expression of fibroblast growth factor 19 (Fgf19) during chicken embryogenesis and eye development, compared with Fgf15 expression in the mouse. *Gene Expr Patterns*. 2004;4(6):687-693. https://doi.org/10.1016/j.modgep.2004.04.005
88. Fredriksson L, Li H, Eriksson U. The PDGF family: four gene products form five dimeric isoforms. *Cytokine Growth Factor Rev*. 2004;15(4):197-204. https://doi.org/10.1016/j.cytogfr.2004.03.007
89. Orr-Urtreger A, Lonai P. Platelet-derived growth factor-A and its receptor are expressed in separate, but adjacent cell layers of the mouse embryo. *Development*. 1992;115(4):1045-1058.
90. Yu FX, Zhao B, Guan KL. Hippo pathway in organ size control, tissue homeostasis, and cancer. *Cell*. 2015;163(4):811-828. https://doi.org/10.1016/j.cell.2015.10.044
91. Cordenonsi M, Zanconato F, Azzolin L, et al. The hippo transducer TAZ confers cancer stem cell-related traits on breast cancer cells. *Cell*. 2011;147(4):759-772. https://doi.org/10.1016/j.cell.2011.09.048
92. Halder G, Johnson RL. Hippo signaling: growth control and beyond. *Development*. 2011;138:9-22. https://doi.org/10.1242/dev.045500
93. Wada KI, Itoga K, Okano T, Yonemura S, Sasaki H. Hippo pathway regulation by cell morphology and stress fibers. *Development*. 2011;138(18):3907-3914. https://doi.org/10.1242/dev.070987

94. Li Z, Wang Y, Zhu Y, et al. The hippo transducer TAZ promotes epithelial to mesenchymal transition and cancer stem cell maintenance in oral cancer. *Mol Oncol*. 2015;9(6):1091-1105. https://doi.org/10.1016/j.molonc.2015.01.007
95. Love MI, Huber W, Anders S. Moderated estimation of fold change and dispersion for RNA-seq data with DESeq2. *Genome Biol*. 2014;15(12):550. https://doi.org/10.1186/s13059-014-0550-8
96. Brawand D, Soumillon M, Necsulea A, et al. The evolution of gene expression levels in mammalian organs. *Nature*. 2011;478(7369):343-348. https://doi.org/10.1038/nature10532
97. Young MD, Wakefield MJ, Smyth GK, Oshlack A. Gene ontology analysis for RNA-seq: accounting for selection bias. *Genome Biol*. 2010;11(2):R14. https://doi.org/10.1186/gb-2010-11-2-r14
98. Lopez-Delisle L, Rabbani L, Wolff J, et al. pyGenomeTracks: reproducible plots for multivariate genomic data sets. *Bioinformatics*. 2021;37(3):422-433. https://doi.org/10.1093/bioinformatics/btaa692
99. Ramírez F, Bhardwaj V, Arrigoni L, et al. High-resolution TADs reveal DNA sequences underlying genome organization in flies. *Nat Commun*. 2018;9(1):1-15. https://doi.org/10.1038/s41467-017-02525-w

How to cite this article: Fernandez-Guerrero M, Zdral S, Castilla-Ibeas A, Lopez-Delisle L, Duboule D, Ros MA. Time-sequenced transcriptomes of developing distal mouse limb buds: A comparative tissue layer analysis. *Developmental Dynamics*. 2022;251(9):1550-1575. https://doi.org/10.1002/dvdy.394